

The Impact of Multisatellite Data on the Initialization and Simulation of Hurricane Lili's (2002) Rapid Weakening Phase

XIAOYAN ZHANG AND QINGNONG XIAO

National Center for Atmospheric Research, Boulder, Colorado*

PATRICK J. FITZPATRICK

GeoResources Institute, Mississippi State University, Stennis Space Center, Mississippi

(Manuscript received 15 November 2005, in final form 19 April 2006)

ABSTRACT

Numerical experiments have been conducted to examine the impact of multisatellite data on the initialization and forecast of the rapid weakening of Hurricane Lili (in 2002) from 0000 UTC to landfall in Louisiana on 1300 UTC 3 October 2002. Fifth-generation Pennsylvania State University–National Center for Atmospheric Research (PSU–NCAR) Mesoscale Model (MM5) 4DVAR sensitivity runs were conducted separately with QuikSCAT surface winds, the *Geostationary Operational Environmental Satellite-8* (*GOES-8*) cloud drift–water vapor winds, and *Aqua* Moderate Resolution Imaging Spectroradiometer (MODIS) temperature–dewpoint sounding data to investigate their individual impact on storm track and intensity. The results were compared against a simulation initialized from a Global Forecast System background interpolated to the MM5 grid. Assimilating QuikSCAT surface wind data improves the analyzed outer-core surface winds, as well as the inner-core low-level temperature and moisture fields. Substantial adjustments of winds are noted on the periphery of the hurricane by assimilating *GOES-8* satellite-derived upper-level winds. Both track forecasts initialized at 1200 UTC 2 October 2002 with four-dimensional variational data assimilation (4DVAR) of QuikSCAT and *GOES-8* show improvement compared to those initialized with the model background. Assimilating *Aqua* MODIS sounding data improves the outer-core thermodynamic features. The *Aqua* MODIS data has a slight impact on the track forecast, but more importantly shows evidence of impacting the model intensity predicting by retarding the incorrect prediction of intensification. All three experiments also show that bogusing of an inner-core wind vortex is required to depict the storm's initial intensity.

To properly investigate Lili's weakening, data assimilation experiments that incorporate bogusing vortex, QuikSCAT winds, *GOES-8* winds, and *Aqua* MODIS sounding data were performed. The 4DVAR satellite-bogus data assimilation is conducted in two consecutive 6-h windows preceding Lili's weakening. Comparisons of the results between the experiments with and without satellite data indicated that the satellite data, particularly the *Aqua* MODIS sounding information, makes an immediate impact on the hurricane intensity change beyond normal bogusing procedures. The track forecast with the satellite data is also more accurate than just using bogusing alone. This study suggests that dry air intrusion played an important role in Lili's rapid weakening. It also demonstrates the potential benefit of using satellite data in a 4DVAR context—particularly high-resolution soundings—on unusual cases like Hurricane Lili.

1. Introduction

Since there are limited conventional observations over the ocean where hurricanes occur and evolve, ef-

fective use of remote sensing data from satellite is crucial for improving hurricane initialization and simulation (Zou and Xiao 2000; Zou et al. 2001; Pu et al. 2002). Data assimilation is a promising technique for using satellite data in the initial conditions of a numerical weather forecast. The technique has improved rapidly in the 1990s, but has stagnated somewhat in recent years. An area of interest in data assimilation now is how to properly and effectively assimilate current large amounts of satellite data available at unprecedented resolutions. It is possible to accelerate this key problem through exploring some unusual hurricane cases, espe-

* The National Center for Atmospheric Research is sponsored by the National Science Foundation.

Corresponding author address: Dr. Qingnong Xiao, National Center for Atmospheric Research, Mesoscale and Microscale Meteorology Division, P.O. Box 3000, Boulder, CO 80307-3000.
E-mail: hsiao@ucar.edu

cially those not predicted well by operational centers. This study focuses on the rapid weakening of Hurricane Lili over the Gulf of Mexico beginning early on 3 October 2002. During 0000–1300 UTC 13 October 2002, Hurricane Lili rapidly weakened from category 4 to category 1, with its maximum sustained wind decreasing by 45 kt in the 13-h period until making landfall in Louisiana. Operational models failed to predict this rapid weakening. However, until now, this rapid weakening process just before landfall is still not well understood. Frederick (2003) showed that Lili's weakening rate over water ranks the hurricane in the first percentile when compared with 769 other hurricanes in the historical database, and it is also the only hurricane to have decayed at a greater rate than it intensified. The collapse of this system needs further investigation.

Satellite datasets preceding Lili's rapid weakening period include QuikSCAT surface winds, *Geostationary Operational Environmental Satellite-8 (GOES-8)* cloud drift/water vapor winds, and *Aqua* Moderate Resolution Imaging Spectroradiometer (MODIS) temperature–dewpoint sounding data. QuikSCAT refers to the National Aeronautics and Space Administration (NASA) mission that utilizes the SeaWinds scatterometer; this instrument uses pencil-beam antennas in a conical scan that radiate Ku-band microwaves at 46° and 54° incident angles and measure backscatter power along a 1800-km swath, deriving 10-m wind speed and direction at 25-km resolution in clear and nonprecipitating cloudy conditions (Graf et al. 1998). QuikSCAT winds can improve analysis and forecasts of hurricanes through better depiction of their outer-core surface wind field, and generally have an accuracy of 10% or 2 m s^{-1} , depending on which is larger, and directional accuracy of 20°, for wind ranges of 3–30 m s^{-1} . Brown and Zeng (1994) showed that surface pressure analyses derived from the *European Remote Sensing Satellite-1 (ERS-1)* winds capture many details not present in the European Centre for Medium-Range Weather Forecasts (ECMWF) operational analysis. Katsaros et al. (2001) demonstrated that QuikSCAT provide valuable information about ambient surface wind fields in which tropical cyclones were embedded. Leidner et al. (2003) showed that assimilating the NASA Scatterometer (NSCAT) wind data by the four-dimensional variational data assimilation (4DVAR) improved the 2–5-day forecast track, as well as storm's thermodynamic structure.

Recent studies show that satellite cloud drift–water vapor winds have a positive impact on tropical forecasting (Le Marshall et al. 1985; Mills et al. 1986; Velden et al. 1992, 1998; Soden et al. 2001). These datasets are generated by the tracking of persistent, identifiable

cloud or water vapor features in GOES satellite imagery to provide an estimation of the ambient wind flow. The utilization of satellite-derived upper winds improved model track forecasts in: the Tropical Cyclone Motion field program (Elsberry 1990); the northwest Pacific (Bennett et al. 1993; Xiao et al. 2002); and Tropical Cyclone Rewa in the Coral Sea (Le Marshall et al. 1996). The work of Bennett et al. (1993) has now been extended from barotropic to full baroclinic models in the context of a 4DVAR assimilation procedure (Bennett et al. 1996), which also supported improved hurricane track forecasts. More recent examples where high-density satellite-derived winds decreased track errors include Leslie et al. (1998) and Velden et al. (1998). Model vertical velocity fields are also improved using upper-level satellite winds, as shown in Zou and Xiao (2000) for Hurricane Felix (1995).

Satellite-derived temperature–dewpoint sounding data are available from MODIS on NASA's *Aqua* satellite. The *Aqua* MODIS atmospheric profile algorithm is a statistical regression with the option for a subsequent nonlinear physical retrieval. The retrievals are performed using clear-sky radiances measured by MODIS with an approximate 5-km resolution over land and ocean for both day and night (Menzel et al. 2002; King et al. 2003). Each retrieved sounding maps temperature and dewpoint to 20 pressure levels ranging from 1000 to 5 hPa. As a new type of data, however, their impacts have not been fully explored, and there is not much data assimilation research on these data in the literature. The relevant research on assimilation of the retrieval temperature profiles from the Advanced Microwave Sounding Unit (AMSU-A) showed a positive impact on the construction of more realistic vortex in the hurricane initialization (Zhu et al. 2002; Zhao et al. 2005).

The data assimilation system used in this research is the fifth-generation Pennsylvania State University–National Center for Atmospheric Research (PSU–NCAR) Mesoscale Model (MM5) 4DVAR system (Zou et al. 1998). This data assimilation package has successfully incorporated GOES and the Geostationary Meteorological Satellite (GMS) cloud drift/water vapor wind (Xiao et al. 2002), GOES brightness temperature (Zou et al. 2001), the Special Sensor Microwave Imager (SSM/I) precipitation water (Xiao et al. 2000a), GPS precipitable water (Guo et al. 2000), and GPS radial occultation data (Kuo et al. 2000).

The advantage of 4DVAR lies in its ability to assimilate data over a time window using the model as a strong constraint to produce an optimal initialization field. An observation in space and time is controlled by the model dynamics so that information is more realis-

tically spread out. This is the main reason 4DVAR was chosen over 3DVAR, which treats each observation as static information. 4DVAR does have some weaknesses, however, such as using an adjoint of tangent linear model instead of the full Euler–Lagrange equations, and being computationally expensive. In recent year, an ensemble Kalman filter (EnKF) has emerged as a promising data assimilation technique (Evensen 1994; Dowell et al. 2004; Xue et al. 2006). However, because EnKF is more challenging to use, 4DVAR was chosen for this study.

This paper is arranged as follows. A brief overview of Hurricane Lili (in 2002) is given in the following section. Section 3 discusses the satellite-retrieved products. Experimental designs are described in section 4. The initialization and simulation results of data sensitivity experiments and 4DVAR cycling experiments are shown in sections 5 and 6, respectively. Conclusions and future work are discussed in section 7.

2. Overview of Hurricane Lili (in 2002)

Lili originated from an African tropical wave and became a tropical depression on 21 September 900 nm east of the Windward Islands. After becoming a named storm it impacted the Caribbean Sea as a tropical storm, weakened to a tropical wave, and regenerated as a tropical storm and eventual hurricane. It emerged from western Cuba as a hurricane with winds of 90 kt on 1200 UTC 1 October 2002 and a central sea level pressure (CSLP) of 971 hPa. Lili's northwest forward motion then gradually increased to 15 kt, followed by a turn to the north, experiencing rapid intensification with sustained winds increasing from 90 kt (CSLP = 967 hPa) to 125 kt (CSLP = 940 hPa) from 0000 UTC 2 October to 0000 UTC 3 October 2002, just south of central Louisiana. Lili then unexpectedly rapidly weakened in the following 13 h, with winds decreasing to 80 kt (CSLP = 962 hPa) until making landfall on 1300 UTC 3 October 2002. Graphs of the hurricane's best track is shown in Fig. 1a, and the best-track maximum surface wind speed and CSLP reported by the National Hurricane Center (NHC), as a function of time, are shown in Fig. 1b.

3. Observations from satellite-retrieved products

a. QuikSCAT winds

QuikSCAT winds data are available at 1200 UTC 2 October 2002 in the Gulf of Mexico before Hurricane Lili's rapid weakening. The data covers much of the hurricane periphery (Fig. 2). Data within heavy precipi-

tation regions is assumed contaminated and not used. Comparison between QuikSCAT winds and the first-guess winds [the product of the Global Forecast System (GFS) data interpolated to the MM5 grid] demonstrates that QuikSCAT winds generally agree with the MM5 first-guess winds (Fig. 3). The average QuikSCAT wind is about 0.24 m s^{-1} larger than the MM5 first-guess winds.

b. GOES-8 cloud drift–water vapor winds

Five sets of cloud drift–water vapor winds observations are available preceding Lili's weakening period on 1200, 1315, 1645, 1915, and 2215 UTC 2 October 2002. They are distributed over the entire troposphere, but are largely concentrated in the upper troposphere at or above 400 hPa. Quality control was conducted before assimilating the wind data, rejecting data based on flags defined in Holmlund et al. (2001). Figure 4 shows the general agreement between GOES-8 winds and MM5 first-guess winds on all GOES-8 cloud drift–water vapor wind data at 1200, 1315, and 1645 UTC 2 October 2002.

c. Aqua MODIS temperature–dewpoint soundings

Aqua MODIS temperature–dewpoint sounding data are distributed at 1800 and 2000 UTC 2 October 2002. Only data that pass NASA's quality assurance flags are included. These flags largely depend on cloud mask algorithms, since MODIS retrievals require clear-sky measurements. Each pixel is quantified as clear by combining the results of several spectral threshold tests, with a clear-sky confidence level assigned based on a comparison between observed radiances and specified thresholds. The retrieval algorithm requires at least 5 of the 25 pixels in a 5×5 field-of-view area to have been assigned a 95% or greater confidence of clear by the cloud mask. The retrieval for each 5×5 field-of-view area is performed using the average radiance of those pixels that were considered clear. Therefore, the MODIS retrievals are only used outside the cloud canopy of Hurricane Lili. The NASA algorithm may also identify regions with large sensor zenith angles as questionable data.

To assess the reliability of the Aqua MODIS soundings, the satellite data was validated against dropsonde data from Hurricane Lili reconnaissance flights. In general, temperature comparisons are excellent, while moisture measurement have larger differences but are still representative of the moisture profile. Figure 5 shows an example profile at 19.87°N , 83.37°W , comparing a dropsonde observation to a nearby Aqua MODIS sounding profile. A dropsonde temperature deviation

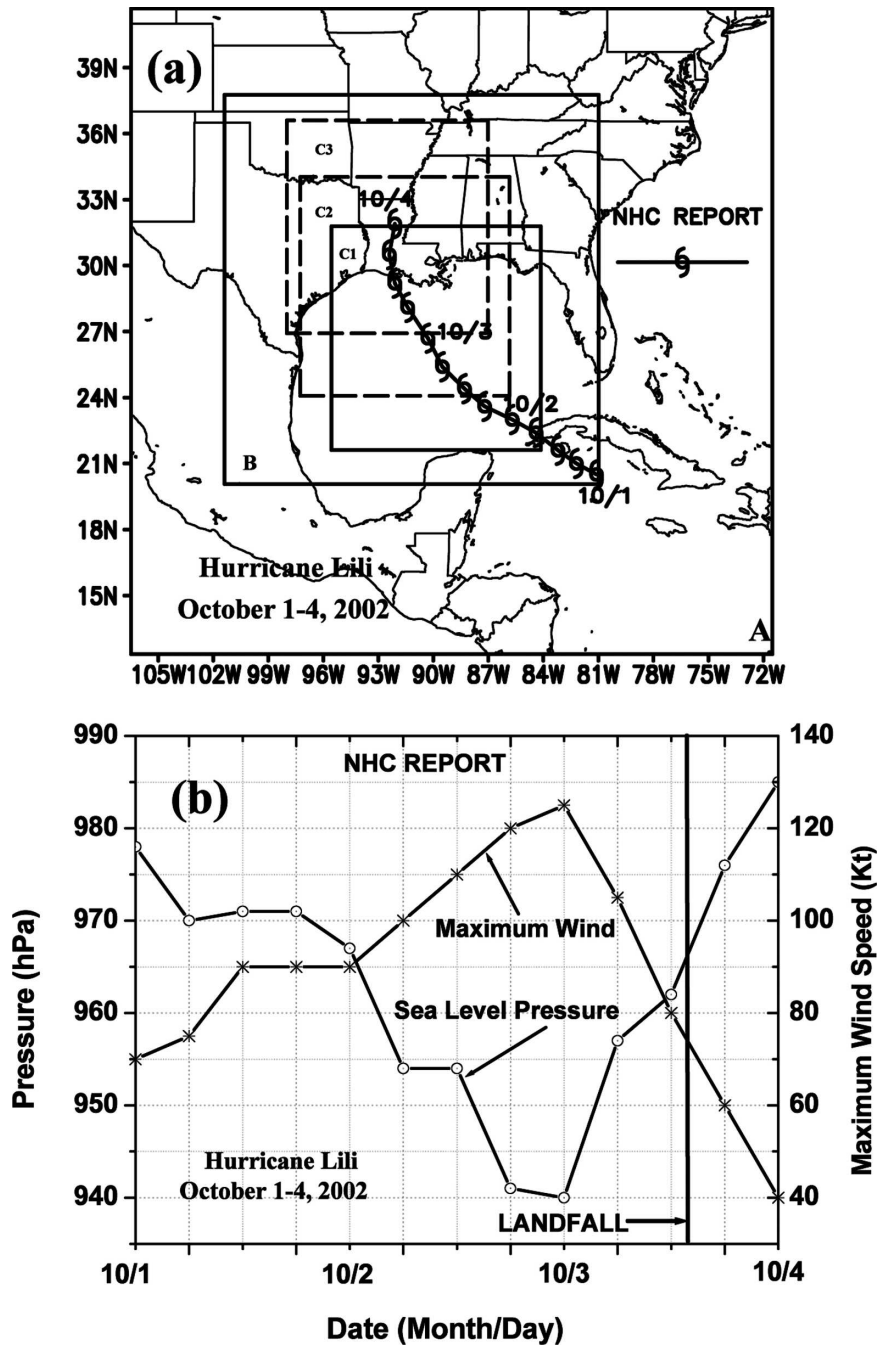


FIG. 1. (a) The NHC best-track positions and (b) CSLP (hPa, circle and solid line) and maximum wind speed (kt, asterisk and solid line) for Hurricane Lili during 1–4 Oct 2002. Landfall occurred at 1300 UTC 3 Oct 2002. The three model domains used for the simulation are presented in (a).

occurs above 200 hPa because the dropsonde is turned on inside the plane before being dropped. Table 1 shows the statistical root-mean-square error (RMSE) in each vertical level, comparing *Aqua* MODIS data versus nine dropsonde profiles. The data above 200 hPa

were discarded in the statistics. The criteria for matching dropsonde and *Aqua* profile were that they have to be within a distance of 0.4° , and within one hour of each other, resulting in 144 *Aqua* soundings. The dropsonde profile is interpolated to the *Aqua* pressure levels using

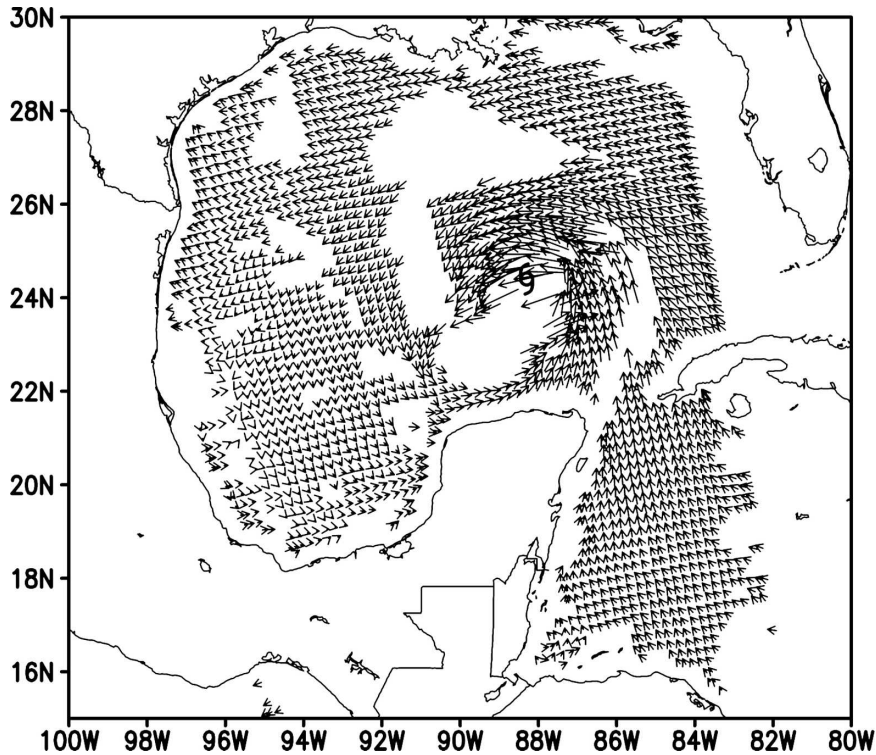


FIG. 2. QuikSCAT wind distribution within MM5 Domain B (85×85 grid, $\Delta x = 27$ km) at 1200 UTC 2 Oct 2002.

an Akima spline routine. This shows generally small RMSE values except for dewpoint in the upper troposphere.

Because the 4DVAR is applied to a 27-km grid spacing, *Aqua's* 5-km profile data is thinned to 30-km resolution. Additional quality control is also performed, rejecting any data with an absolute difference greater than 5°C compared to the background. The dewpoint temperature is converted to specific humidity before assimilation in the 4DVAR scheme.

4. Experiment design

a. MM5 model and 4DVAR

The numerical model used in this study is the non-hydrostatic, movable, triple-nested grid, mesoscale model, MM5. The model consists of 33 layers in the vertical with the model top at 50 hPa. The simulations are triple nested with horizontal resolutions of 81 (domain A), 27 (domain B), and 9 km (domain C). The coarse domain and the intermediate domain are fixed, while the inner domain moves with the hurricane track (Fig. 1a). The (x, y) dimensions are 48×50 , 85×85 , and 142×142 , respectively. The precipitation scheme uses the Dudhia ice scheme for domains A and B, and

the Reisner graupel (Reisner et al. 1998) option for domain C. Cumulus parameterization is performed using Grell for domains A and B, and Betts–Miller for domain C. Boundary layer physics relies on the Blacka-

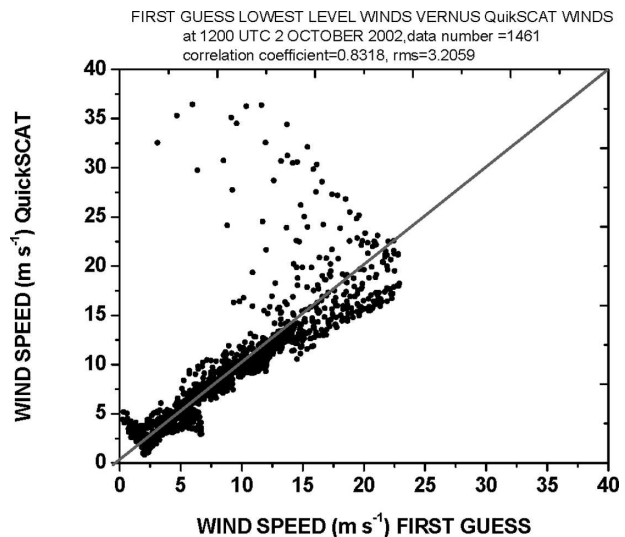
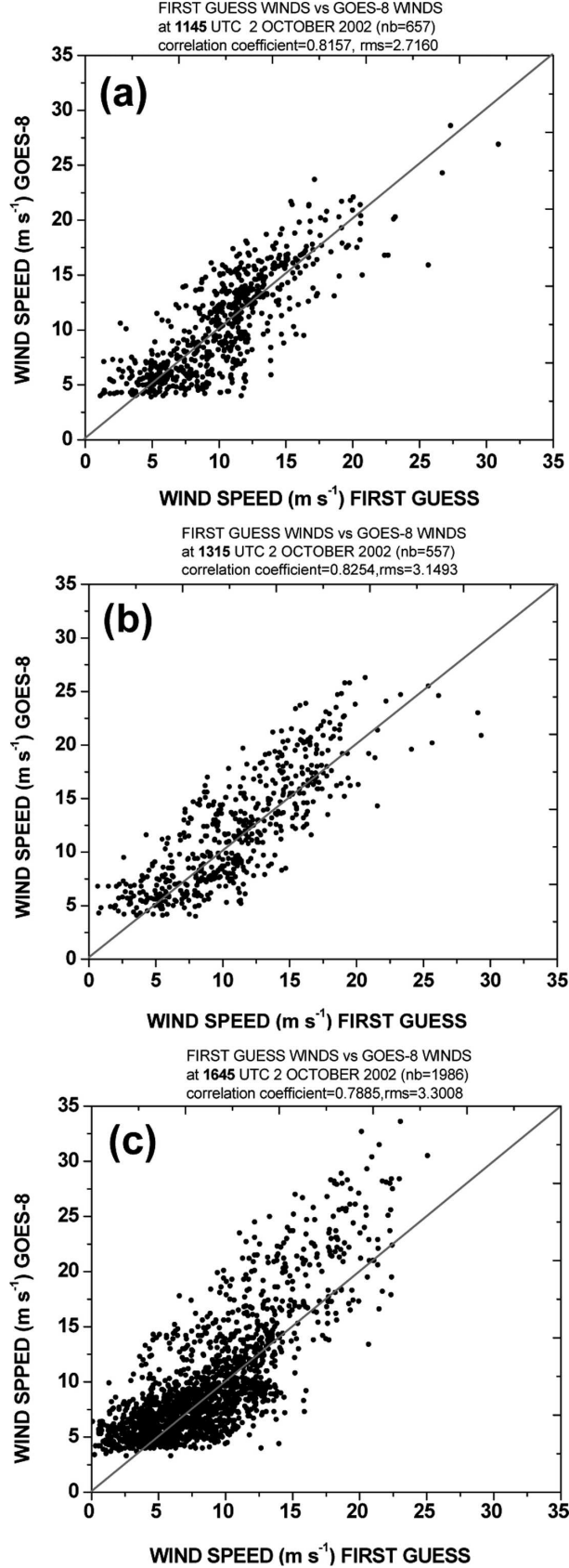


FIG. 3. Scatterplot for QuikSCAT wind speeds and MM5 first-guess wind speeds at 1200 UTC 2 Oct 2002, at the observed location.



dar scheme for all three domains. SST information comes from the NCEP global analysis and is kept unchanged in the model integration.

The NCEP analysis also provides the first-guess fields for the 4DVAR data assimilation experiments, and the initial condition of the control run (CTRL) experiment. While the triple-nested MM5 is used in the numerical forecasts, 4DVAR is performed on a single domain (see sections 4c,d for details). The physical processes that are employed in the MM5 4DVAR system include the Blackadar high-resolution planetary boundary layer scheme, the Grell cumulus scheme, surface friction, surface fluxes, dry convective adjustment, and a large-scale precipitation process that simply removes supersaturation as precipitation and adds the latent heat to the thermodynamic equation.

b. Definition of cost functions in the 4DVAR formulation

The formulation of 4DVAR is based on the perfect model assumption. In this approach, the numerical model is treated as a strong constraint in the formulation for the minimization of a predefined cost function. In this study, we defined the cost function as

$$J = J_B + J_1 + J_2 + J_3 + J_4, \quad (4.1)$$

where

$$J_B = \frac{1}{2} (\mathbf{X} - \mathbf{X}_b)^T \mathbf{B}^{-1} (\mathbf{X} - \mathbf{X}_b), \quad (4.2)$$

$$J_1 = \frac{1}{2} \sum_t \sum_r \{ [\mathbf{u}^{\text{OSCAT}} - \mathbf{H}_t \mathbf{u}]^T \mathbf{W}_{\text{OSCAT}} [\mathbf{u}^{\text{OSCAT}} - \mathbf{H}_t \mathbf{u}] + [\mathbf{v}^{\text{OSCAT}} - \mathbf{H}_t \mathbf{v}]^T \mathbf{W}_{\text{OSCAT}} [\mathbf{v}^{\text{OSCAT}} - \mathbf{H}_t \mathbf{v}] \}, \quad (4.3)$$

$$J_2 = \frac{1}{2} \sum_t \sum_r \{ [\mathbf{u}^{\text{SATW}} - \mathbf{H}_t \mathbf{u}]^T \mathbf{W}_{\text{SATW}} [\mathbf{u}^{\text{SATW}} - \mathbf{H}_t \mathbf{u}] + [\mathbf{v}^{\text{SATW}} - \mathbf{H}_t \mathbf{v}]^T \mathbf{W}_{\text{SATW}} [\mathbf{v}^{\text{SATW}} - \mathbf{H}_t \mathbf{v}] \}, \quad (4.4)$$

$$J_3 = \frac{1}{2} \sum_t \sum_r \{ [\mathbf{t}^{\text{TERRA}} - \mathbf{H}_t \mathbf{t}]^T \mathbf{W}_t [\mathbf{t}^{\text{TERRA}} - \mathbf{H}_t \mathbf{t}] + [\mathbf{q}^{\text{AQUA}} - \mathbf{H}_t \mathbf{q}]^T \mathbf{W}_q [\mathbf{q}^{\text{AQUA}} - \mathbf{H}_t \mathbf{q}] \}, \quad (4.5)$$

←

FIG. 4. Scatterplot for GOES-8 winds speed and MM5 first-guess winds speeds at (a) 1145, (b) 1315, and (c) 1645 UTC 2 Oct 2002, at the observed location.

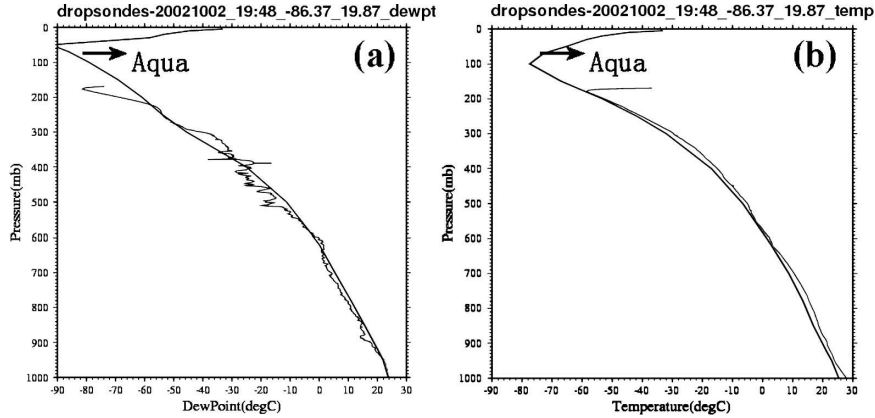


FIG. 5. Comparison of an *Aqua*-retrieved (a) dewpoint temperature and (b) temperature soundings within 0.4° of a hurricane reconnaissance dropsonde profile located at 19.87°N , 83.37°W at 1948 UTC 2 Oct 2002. The dropsonde observation above 200 hPa reflects readings inside the aircraft before being ejected from the plane, and should be disregarded.

and

$$J_4 = \frac{1}{2} \sum_t \sum_\Omega [\mathbf{P}_0^{\text{bogus}}(r) - \mathbf{P}(r)]^T \mathbf{W}_p [\mathbf{P}_0^{\text{bogus}}(r) - \mathbf{P}(r)] + \sum_t \sum_\Omega \sum_k \{[\mathbf{V}_0(r, k) - \mathbf{V}(r, k)]^T \mathbf{W}_v [\mathbf{V}_0(r, k) - \mathbf{V}(r, k)]\}. \quad (4.6)$$

Here J_B is the background term of the cost function and J_1, J_2 , and J_3 represent the observation terms of the cost function from the QuikSCAT winds, *GOES-8* winds, and *Aqua* temperature and specific humidity terms, respectively. The hurricane bogus data assimilation (BDA) is also included in the data assimilation design, and the related bogus observation term in the cost function is presented in J_4 , which has the bogus sea level pressure (SLP) and wind profiles. The \mathbf{H}_i in Eqs. (4.3)–(4.5) is the linear interpolation operator from model space to observation space. In J_3 , q is calculated from dewpoint temperature ($^\circ\text{C}$) following the Magnus formulation using Tetens's constants (Elliott and Gaffen 1993):

$$e = 6.1078 \times 10^{[(Td \times A)/(Td + B)],}$$

where $A = 7.5$, $B = 237.3$, and $q = (0.622e)/(p - 0.378e)$.

(4.7)

In J_4 , P_0 and V_0 are specified according to the BDA

scheme (Xiao et al. 2000b) by the following equations (Fujita 1952):

$$P_0(r) = p_c + \Delta p \left\{ 1 - \left[1 + \frac{1}{2} \left(\frac{r}{R_m} \right)^{-1/2} \right] \right\}, \quad (4.8)$$

and

$$V_0(r) = \left(\frac{r}{\rho} \frac{\partial p_0}{\partial r} + \frac{f^2 r^2}{4} \right)^{1/2} - \frac{r|f|}{2}, \quad (4.9)$$

where p_c is the hurricane CSLP, $\Delta p = (p_{\text{env}} - p_c)$, and p_{env} is the environment surface pressure. Here R_m is the estimated radius of the maximum surface wind, and r is the radial distance from the cyclone center. For Hurricane Lili, p_c is 954 hPa at 1200 UTC and 941 hPa at 1800 UTC 2 October 2002; and R_m is 78 and 72 km, respectively at 1200 and 1800 UTC 2 October 2002. Air density ρ is assumed a constant. The vertical wind profile has a weighting distribution of 1.0, 1.0, 0.95, 0.85, 0.65, and 0.35 at the corresponding 1000-, 850-, 700-, 500-, 400-, and 200-hPa levels (Xiao et al. 2000b). Pu and Braun (2001) showed this technique ensures gradient wind balance, which produces a better vortex structure and prevents vortex spindown problems. Zhang et al. (2003) also evaluated this method in a typhoon case study. Leslie and Holland (1995) have pointed out the dangers of using a bogus, since the tropical cyclone track is very sensitive to the choice of radius and maximum wind. In the 4DVAR context, this problem is specified as a weighted least squares constraint that will

TABLE 1. RMSE of *Aqua* MODIS temperature–dewpoint soundings vs dropsondes ($^\circ\text{C}$).

Level (hPa)		1000	950	920	850	780	700	620	500	400	300	250	200
RMS	Temperature	1.04	1.08	0.93	0.86	0.70	1.27	1.58	0.84	1.29	1.60	0.70	1.39
Error	Dewpoint	1.46	1.03	2.04	2.81	1.95	1.98	4.28	2.97	3.53	4.09	6.88	7.26

TABLE 2. Description of data sensitivity experiments for 2 Oct 2002.

Expt	Window	Start time (UTC)	Domain	Data type	Data time (UTC)
QSCAT	0.5 h	1200	B	QuikSCAT winds	1200
SATW	5 h	1200	A	GOES-8 winds	1200, 1315, 1645
AQUA	2 h	1200	B	Aqua soundings	1800, 2000

most certainly assist in minimizing the dependence on the bogus vortex chosen.

The background error covariance matrix \mathbf{B} is estimated from the difference between the MM5 forecast and the NCEP analysis. The observation weightings in the cost function are treated as constants and determined empirically as $W_{\text{QSCAT}} = 25 \text{ s}^2 \text{ m}^{-2}$, $W_{\text{SATW}} = 50 \text{ s}^2 \text{ m}^{-2}$, $W_p = 100 \text{ hPa}^{-2}$, and $W_v = 50 \text{ s}^2 \text{ m}^{-2}$. Here W_t is obtained by inverting the RMSE of temperature from Table 1 and W_q is deduced from the RMSE of dewpoint temperature in Table 1, and converted to the equivalent specific humidity RMSE. However, the choice of weights for the minimization process in 4DVAR is always a challenge, and more research is required to adequately define the weights in the hurricane environment.

c. Design of data sensitivity experiments

Three data sensitivity experiments are conducted to examine the individual impact of QuikSCAT winds, GOES-8 retrieved winds, and Aqua MODIS soundings on the initialization and the subsequent forecasts, and reported in section 5. The start time and assimilation window for each experiment depends on the data time (Table 2). These experiments are conducted before the 4DVAR cycling experiments (section 4d) to find out the behavior of each satellite data in the MM5 4DVAR systems. More details about the experiment designs are described in Table 2.

d. 4DVAR cycling experiments

The cycling 4DVAR experiments are conducted over domain B with two consecutive 6-h assimilation windows, labeled as 4DVAR6H1 and 4DVAR6H2, and reported in section 6. 4DVAR6H1 assimilates data from 1200 to 1800 UTC 2 October 2002, and 4DVAR6H2 extends from 1800 UTC 2 October to 0000 UTC 3 October 2002. Then, the model simulation commences, matching the period when Lili underwent rapid weakening. In 4DVAR6H1, the first-guess field is the same as the initial condition of CTRL, while in 4DVAR6H2 the optimal solution (assimilation results) at the end of 4DVAR6H1 is used as the first guess. Note that the assimilation results from 4DVAR6H1 affect the results of 4DVAR6H2.

4DVAR6H1 assimilates QuikSCAT winds at 1200 UTC, GOES-8 cloud drift/water vapor winds at 1145, 1315, and 1645 UTC, and a bogus vortex at 1200 UTC 2 October 2002, while 4DVAR6H2 assimilates GOES-8 cloud drift–water vapor winds at 1915 and 2215 UTC, Aqua MODIS soundings at 1800 and 2000 UTC, and the bogus vortex at 1800 UTC 2 October 2002. To examine the satellite data impact, other two 4DVAR cycling experiments are conducted. One denies all satellite data but keeps the BDA of Zou and Xiao (2000), and the other keeps all satellite data but

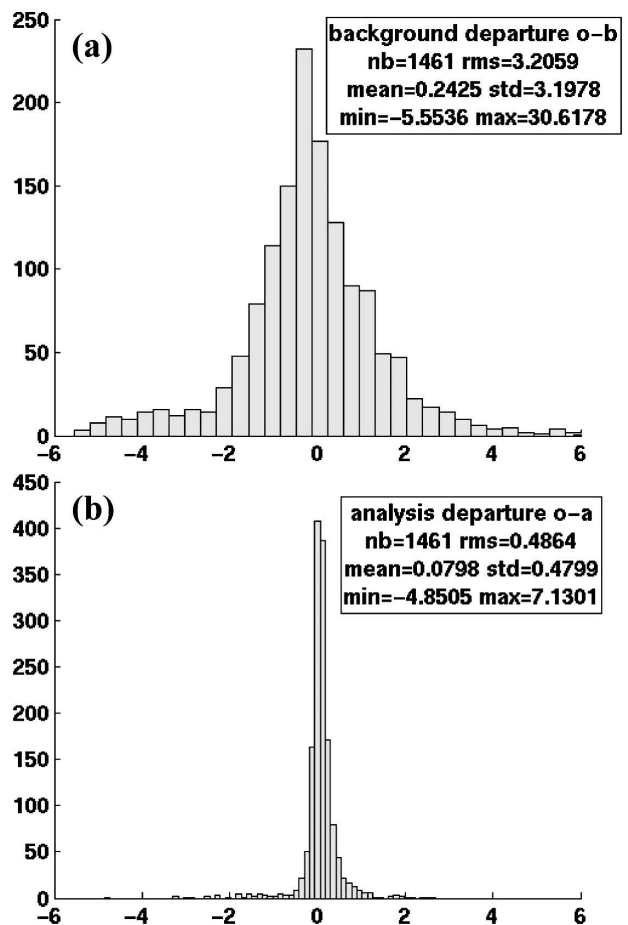


FIG. 6. Histogram of wind speed departures of QuikSCAT observations from (a) MM5 first-guess winds ($o - b$) and (b) MM5 4DVAR analyzed winds ($o - a$) for domain B (27-km grid spacing) at 1200 UTC 2 Oct 2002.

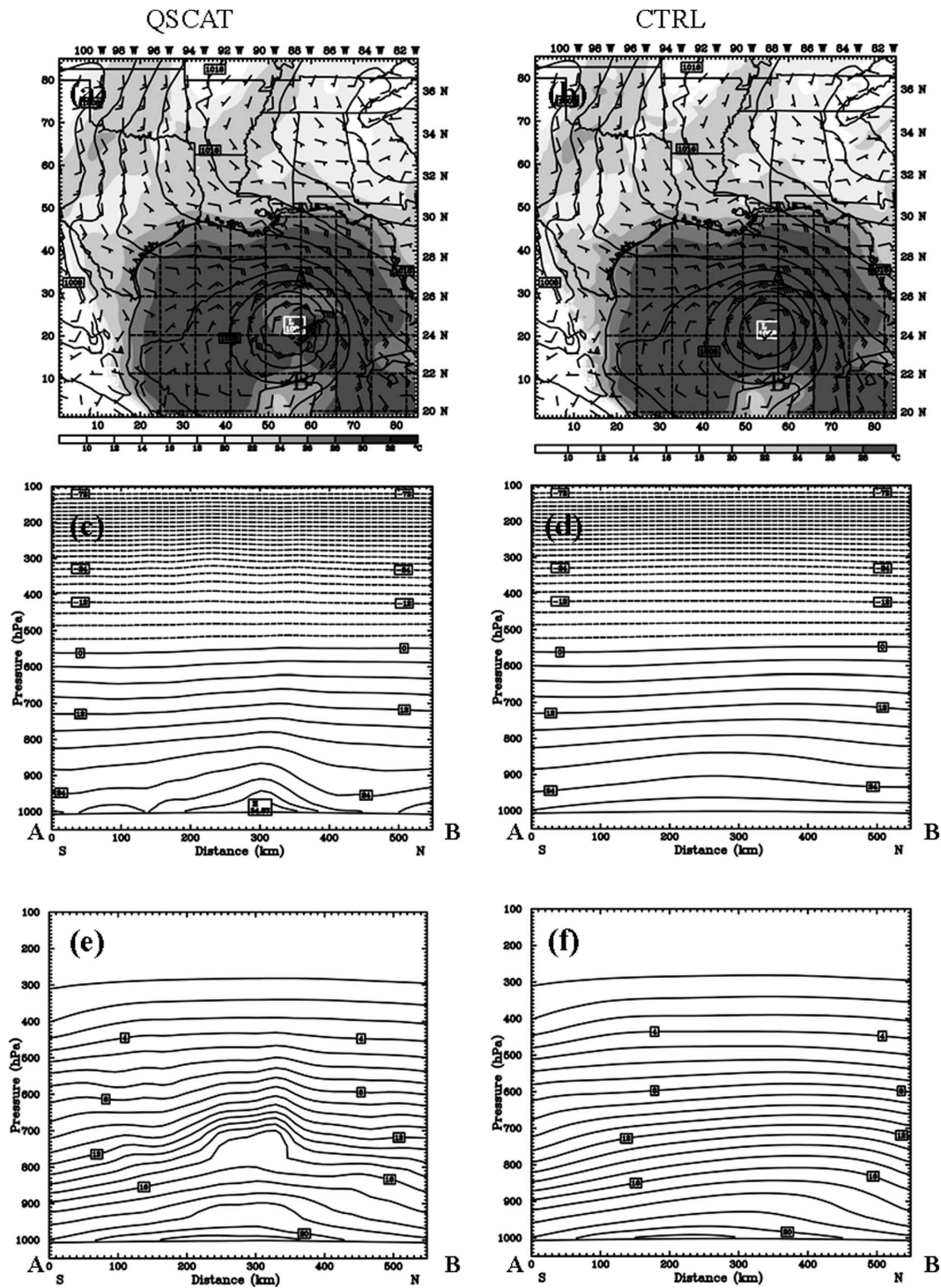


FIG. 7. Winds (m s^{-1}), hurricane CSLP (hPa, contour); and temperature (shading) at 1200 UTC 2 Oct 2002 for (a) QSCAT and (b) CTRL; vertical cross section of temperature ($^{\circ}\text{C}$) for (c) QSCAT and (d) CTRL; vertical cross section of specific humidity (g kg^{-1}) for (e) QSCAT and (f) CTRL.

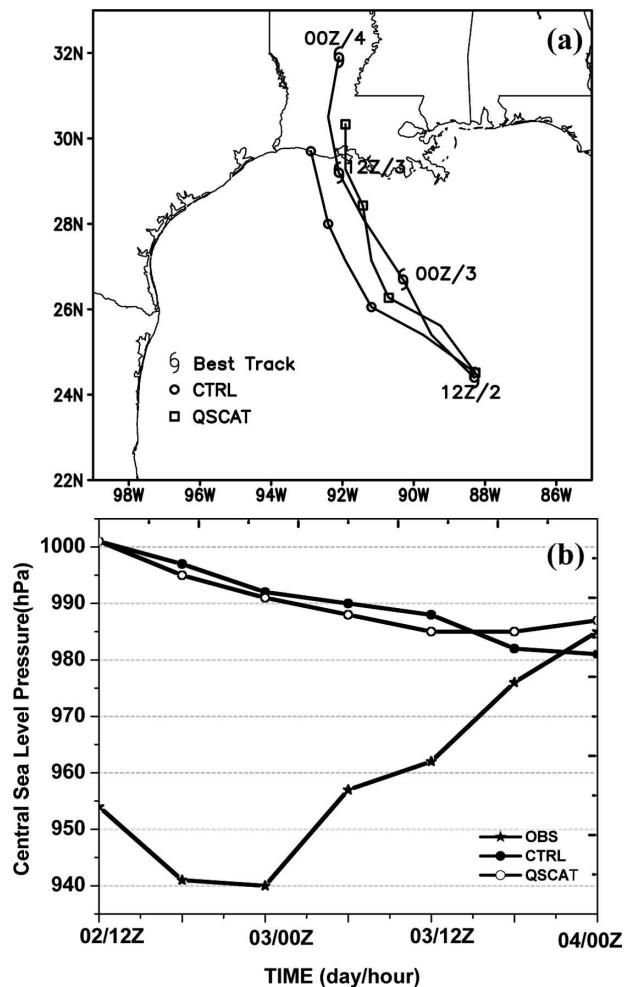


FIG. 8. The 36-h predicted (a) tracks and (b) intensity [CSLP (hPa)] of Hurricane Lili by CTRL and QSCAT initialized at 1200 UTC 2 Oct 2002. The observed track and intensity is shown for comparison.

denies the bogus vortex. In the following discussion, SATC is used as the experiment with aforementioned satellite data during two 6-h assimilation cycles plus bogusing (4DVAR6H1 and 4DVAR6H2); BDAC refers to the 4DVAR cycling that only contains the bogusing (no satellite data); and SATO represents the experiment assimilating all satellite data in the 4DVAR cycling but without vortex bogusing. All forecasts use the triply nested MM5 with a movable domain C (Fig. 1a). The initial conditions of domain C are interpolated from domain B.

5. Impact of each individual satellite dataset—Data sensitivity experiments

a. QuikSCAT data sensitivity study

A total of 1461 QuikSCAT observations are assimilated into the initial condition by 4DVAR in the Quik-

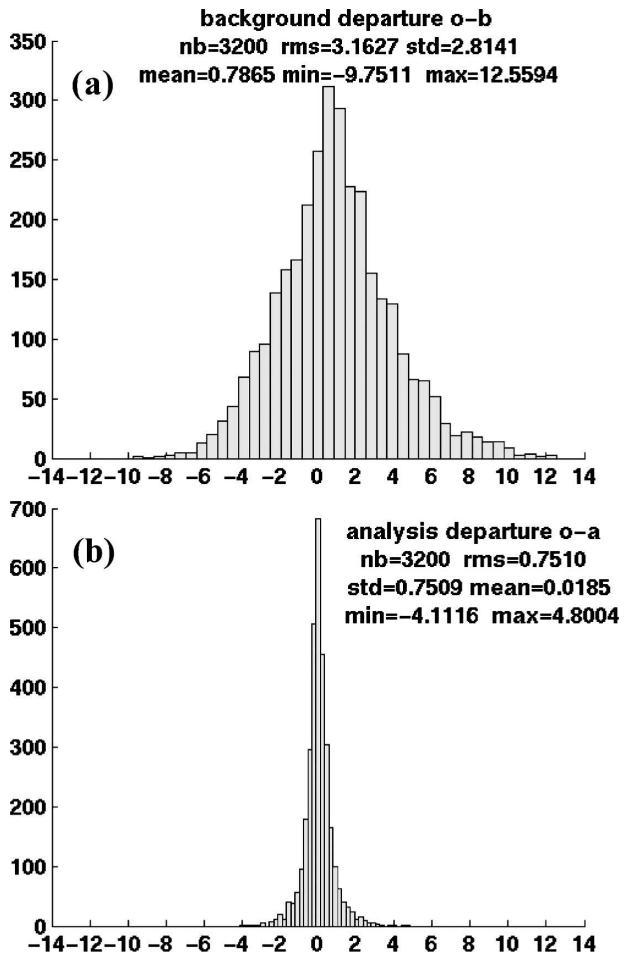


FIG. 9. Histogram of wind speed departures of observations from (a) MM5 first-guess winds ($o - b$) and (b) MM5 4DVAR-analyzed winds ($o - a$) after assimilating *GOES-8* retrieved winds data at 1145, 1315, and 1645 UTC 2 Oct 2002. The assimilation is performed on the coarse domain to effectively include the synoptic-scale environment.

SCAT data sensitivity experiment (QSCAT in Table 2). Figure 6 shows histograms of wind speed departures from the first guess ($o - b$, Fig. 6a) and the analysis ($o - a$, Fig. 6b). The mean departure of $o - a$ (0.0798) is 3 times smaller than $o - b$ (0.2425). The $o - b$ RMSE of 3.2059 reduces to 0.4864 for $o - a$. The 4DVAR produces analyses that fit the QuikSCAT observations very well.

The assimilation of QuikSCAT wind data has an obvious improvement in the 1200 UTC analysis, as shown in Fig. 7. Comparing Figs. 7a with 7b, assimilating QuikSCAT wind data improve not only the initial surface wind, but also the temperature at the lower levels. The increase of the surface cyclonic wind speed strengthens the low-level convergence, initiating stronger updrafts and releasing more latent heat. A stronger vortex also more efficiently converts diabatic heating to inner-core

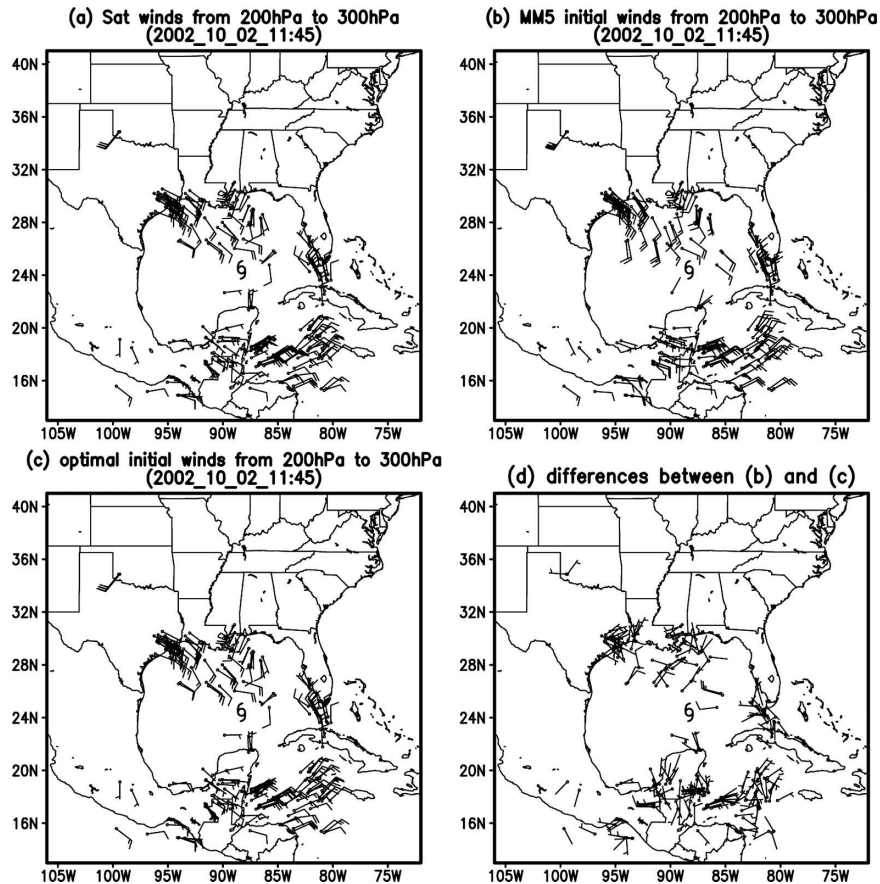


FIG. 10. (a) *GOES-8* retrieved winds at 1145 UTC 2 Oct 2002 between 200 and 300 hPa, (b) original initial winds from MM5 background at 1200 UTC 2 Oct 2002, (c) optimal initial winds from 4DVAR, and (d) the difference between (b) and (c).

warming during the gradient wind adjustment process, since less of the latent heat can travel away as gravity waves (Hack and Schubert 1986). The maximum temperature at the model's lowest level is 33°C within the hurricane center after QuikSCAT wind data assimilation (Fig. 7a). In contrast, the background analysis (CTRL run) presents a flat temperature field over the entire hurricane area with a temperature of 28°C. A cross section of temperature shows the QuikSCAT assimilation also influences the thermal structure of the boundary layer and lower troposphere (see Fig. 7c versus Fig. 7d). The moisture field is also adjusted below 500 hPa due to the increased convergence after assimilating the QuikSCAT winds; the specific humidity at 700 hPa is 14 g kg⁻¹ in experiment QSCAT (Fig. 7e), but only 11 g kg⁻¹ at the same level in the MM5 analysis (Fig. 7f). This demonstrates that assimilation of the surface QuikSCAT winds in MM5 4DVAR can dynamically adjust the thermal and moisture structure of the storm.

Numerical simulation for this experiment (QSCAT)

is conducted for 36 h, starting from 1200 UTC 2 October 2002. Results show that inclusion of QuikSCAT winds in the initial conditions improves the forecast of the storm track compared to the CTRL experiment (Fig. 8a). The storm track is closer to the best track than CTRL, and the movement speed is also improved. However, the inclusion of QuikSCAT data is not enough to improve the intensity prediction (Fig. 8b). The maximum wind speed after QuikSCAT assimilation is only 35 m s⁻¹, which is much lower than the observed maximum wind speed (56 m s⁻¹) at initialization time. Since the surface wind analysis is too weak, the intensity prediction cannot be improved.

b. Sensitivity of *GOES-8* retrieved winds

SATW described in Table 2 examines the impact of *GOES-8* cloud drift/water vapor winds on the initialization and simulation of Hurricane Lili. The assimilation is performed on the coarse domain to effectively include the synoptic-scale environment. The 4DVAR iterative process improves the analysis compared to the

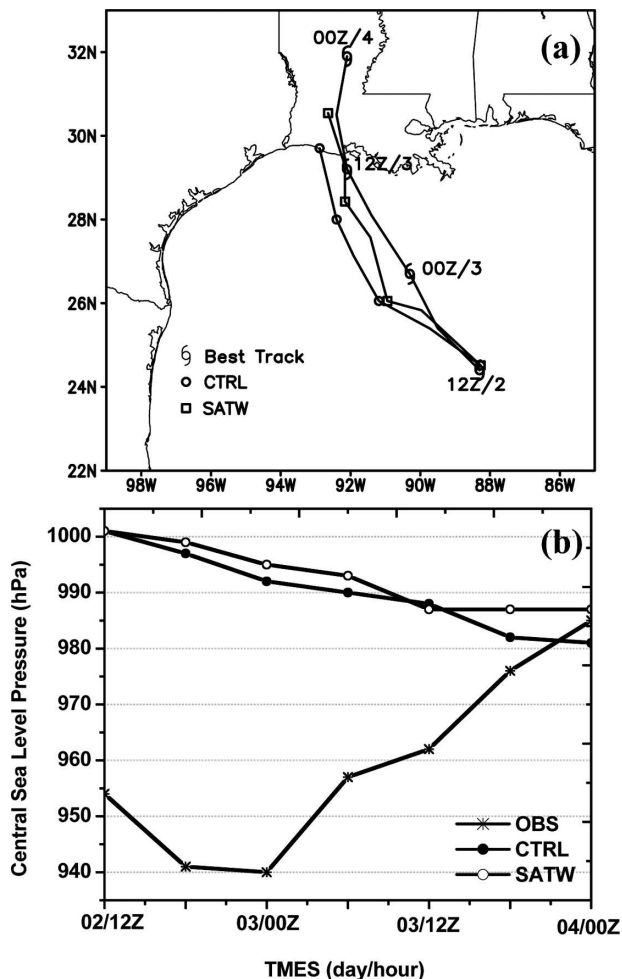


FIG. 11. Same as in Fig. 8, but by CTRL and SATW.

first-guess field, with a narrower spread in the departure field. There are approximately 700 data points with the departure close to zero ($o - a$, Fig. 9b) compared to 300 in the background field ($o - b$, Fig. 9a).

Figure 10 shows that the *GOES-8* winds are successfully assimilated into the initial conditions in SATW. The results of the 4DVAR assimilation of 1145, 1315, and 1645 UTC *GOES-8* winds are shown in Fig. 10c, and the difference field compared with the background in Fig. 10d. Substantial adjustments are noted in some regions, with the optimized winds (Fig. 10c) closer to the observation (Fig. 10a) than the first guess (Fig. 10b). Similar results occur at all levels and other times (figures omitted).

A numerical simulation is conducted to examine the impact of upper-level *GOES-8* winds on the prediction of the hurricane track and intensity. Figure 11a shows the predicted hurricane tracks of Lili by CTRL and SATW, starting from 1200 UTC 2 October 2002. The

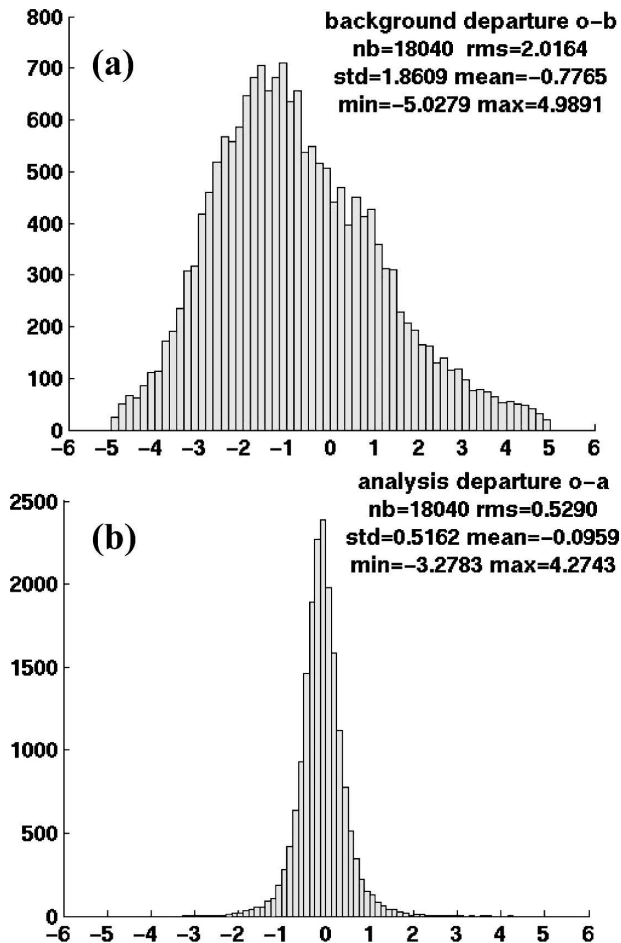


FIG. 12. Histogram of temperature departures of observations at 2000 UTC 2 Oct 2002 from (a) MM5 first-guess temperature ($o - b$) and (b) MM5 4DVAR-analyzed temperature ($o - a$) after assimilating *Aqua* soundings at 1800 and 2000 UTC.

observed best track is also plotted for comparison. The CTRL-simulated hurricane track is west of the observed track and too slow, with a 10-h delay in landfall. In the first 12 h, Lili's movement predicted by SATW is similar to CTRL. In the second 12 h, however, the SATW track turns east, matching the observed track better with a translation speed faster than CTRL. The errors in both the movement and landing time of SATW are reduced significantly. This demonstrates that assimilation of the *GOES-8* satellite winds positively impacts the hurricane track prediction. Concerning the hurricane intensity (Fig. 11b), the CSLP of SATW has the same value as CTRL at the initial time, which is not improved by inclusion of satellite winds. Since the SATW vortex is too weak, the intensity prediction is not improved (Fig. 11b). One possible reason is that the *GOES-8* retrieved winds are sparse in the vicinity of the hurricane center and below 400 hPa.

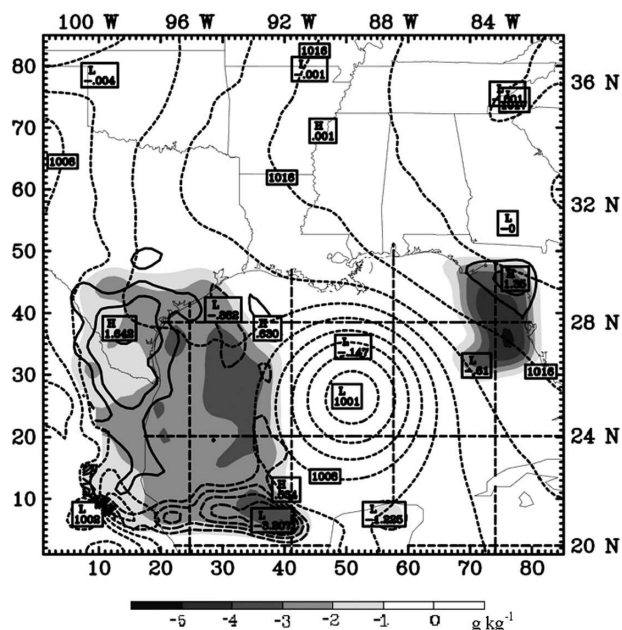


FIG. 13. SLP (short dashed contour, hPa) for 1800 UTC 2 Oct 2002 after assimilating *Aqua* data. Also shown are 850-hPa differences of water vapor mixing ratio (shading, g kg^{-1}) and temperature (solid and long dashed contour, $^{\circ}\text{C}$) between the background field (CTRL) and *Aqua* data assimilation (AQUA).

There is not enough data to properly define the vortex structure that is important for the subsequent intensity prediction.

c. *Aqua* data sensitivity study

An experiment that assimilates *Aqua* MODIS temperature/dewpoint sounding data (AQUA in Table 2) starts from 1800 UTC 2 October 2002, not 1200 UTC as in the QSCAT and SATW experiments. As in the other data sensitivity runs, 4DVAR improves the analysis and background departures for temperature are shown in Fig. 12. Ninety percent of $\sigma - a$ is distributed between -2° and 2°C after 4DVAR, while the same percentage has a wider spread from -5° to 5°C for $\sigma - b$.

Figure 13 shows the mean SLP for 1800 UTC 2 October 2002 after assimilating *Aqua* data, as well as the temperature and specific humidity differences between the experiments with and without *Aqua* data assimilation. Obvious low-level differences are noted west of the hurricane. In particular, the low-level moisture field is $2\text{--}4 \text{ g kg}^{-1}$ drier than the background field. The surface temperature is also a little cooler in most of the domain. These 4DVAR analyzed outer-core thermodynamic fields have a small but noticeable impact on a 30-h simulation initialized at 1800 UTC 2 October 2002 (Fig. 14). There is little difference in the prediction of the track (Fig. 14a) and intensity (Fig. 14b) for both

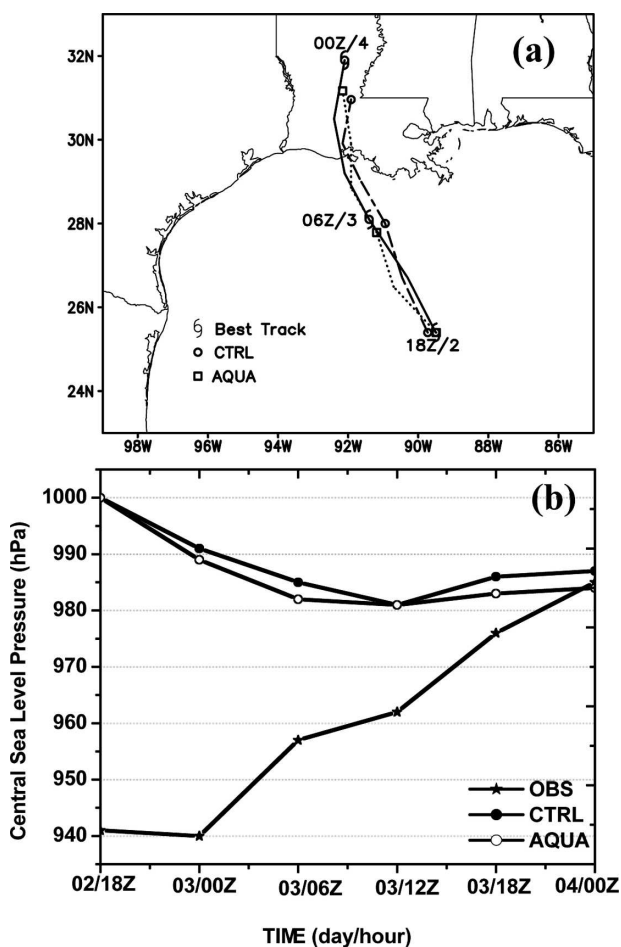


FIG. 14. The 30-h predicted (a) tracks and (b) intensity [CSLP (hPa)] of Hurricane Lili by CTRL, AQUA initialized at 1800 UTC 2 Oct 2002. The observed track and intensity is shown for comparison.

simulations. Since neither run is initialized at the proper intensity due to an inappropriately weak vortex, it's not possible for either to exhibit the correct weakening trend, but the fact the 4DVAR-initialized run quits intensifying suggests that the new thermodynamic information is impacting the model with useful information. To properly investigate the intensity issue, a bogus vortex is necessary in the 4DVAR iterative process. Such experiments are conducted in the next section.

6. Results from 4DVAR cycling experiments

a. Efficiency of MM5 4DVAR

Thirty iterations are performed in the minimization procedure for each 4DVAR experiment per cycle. As expected, the cost function (Fig. 15a) and its gradient (Fig. 15b) for both 4DVAR experiments converge efficiently. This indicates that MM5 4DVAR system has

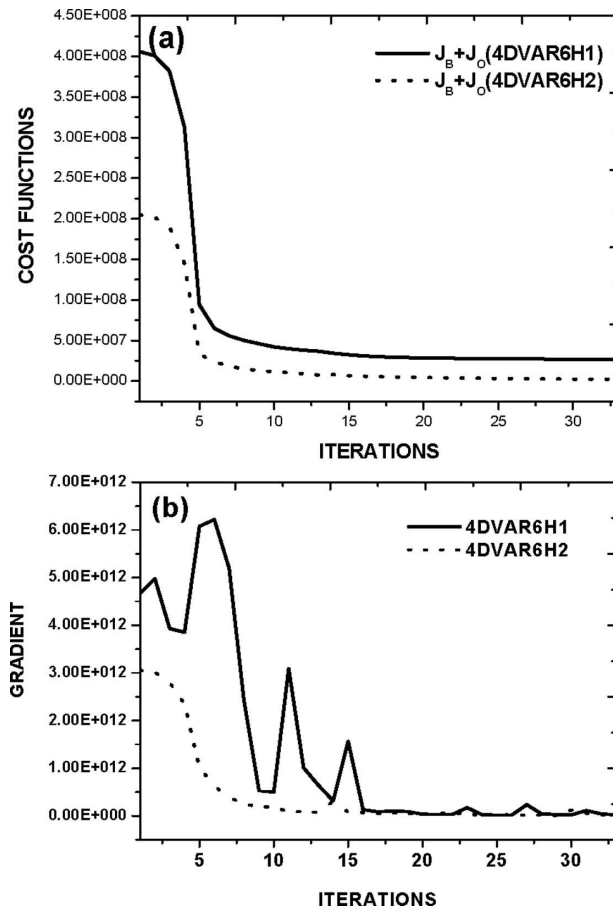


FIG. 15. Variations of (a) cost function terms and (b) gradient terms with respect to iterations for 4DVAR cycling experiment (solid line for 4DVAR6H1, and dotted line for 4DVAR6H2).

the robust ability to assimilate multisatellite data synchronously. However, 4DVAR is a computationally expensive technique, and only a few operational forecast centers have adopted the technique.

b. Optimal initial condition of 4DVAR6H1

In the first 4DVAR cycling experiment (4DVAR6H1), the QuikSCAT winds at 1200 UTC, *GOES-8* cloud drift winds at 1200, 1315, and 1645 UTC, and a bogus vortex at 1200 UTC 2 October 2002 are assimilated over a 6-h time window. Figure 16 shows the SLP and wind analyses for domain C at 1200 UTC (Fig. 16a) after 4DVAR compared with (Fig. 16b) its background field. 4DVAR6H1 is capable of producing the hurricane CSLP of 955 hPa, close to the observed value (954 hPa), while the CSLP is 1002 hPa in the background analysis without any data assimilation. The observed low-level maximum wind speed is 64 m s^{-1} , but only 34 m s^{-1} in the background. After 4DVAR6H1, the low-level maximum wind speed increases by 20 m s^{-1} , but it is still 10 m s^{-1} lower than the observed intensity.

During the minimization procedure in 4DVAR6H1, the temperature and humidity fields are modified by the forward model and its backward adjoint during the assimilation of the wind and pressure data. Figure 17 shows a cross section along the line AB in Fig. 16 for the temperature and humidity fields in 4DVAR6H1, as well as their differences from the background analysis. An approximate 12°C temperature difference is seen in the hurricane's center near the surface (Fig. 17a), and an 8°C difference occurs above 400 hPa. Positive differences of specific humidity are also seen vertically throughout the storm center, with the maximum alteration at 700 hPa (Fig. 17b). These changes are attributed to enhanced boundary layer convergence and a more efficient gradient wind adjustment process as discussed in section 5a.

c. Optimal initial condition of 4DVAR6H2

The analysis at the end of the 6-h assimilation window in 4DVAR6H1 is used as the first guess for 4DVAR6H2 at 1800 UTC 2 October 2002, thereby passing this new information to the next assimilation cycle. 4DVAR6H2 assimilates the *GOES-8* cloud drift winds at 1915 and 2215 UTC, *Aqua* MODIS temperature–dewpoint soundings at 1800 and 2000 UTC, and the bogus vortex at 1800 UTC 2 October 2002. The unique component in this assimilation cycle is the inclusion of the *Aqua* data. Figure 18 depicts the SLP and the lowest level winds, and the north–south cross sections of temperature, humidity, and vertical velocity at 1800 UTC 2 October 2002. The CSLP of 4DVAR6H2 analysis in Fig. 18a is 944 hPa, 3 hPa weaker than observed (941 hPa). Figure 18b shows the temperature field, as well as the deviation relative to the azimuthal average. A warm core above the hurricane surface center is seen, with asymmetries of 2.1°C or less above 800 hPa. The northern eyewall is cooler than the azimuthal mean, while the southern eyewall is warmer than the azimuthal mean. A surface asymmetry of 4.1°C is also seen in the southern eyewall. The low-level specific humidity in the northern eyewall is larger than the southern eyewall (Fig. 18c). Two robust eyewalls convective bands are seen in the vertical motion field, sloping outward with height to 200 hPa (Fig. 18d). The sensitivity to the thermodynamic fields is also apparent, however. The moister northern eyewall boundary layer, combined with the cooler air aloft in the eyewall (which promotes buoyancy), results in strong upper-level vertical motion in the upper eyewall. The warmer southern eyewall boundary layer promotes strong vertical motion near the surface.

At the end of the 4DVAR6H2 assimilation window

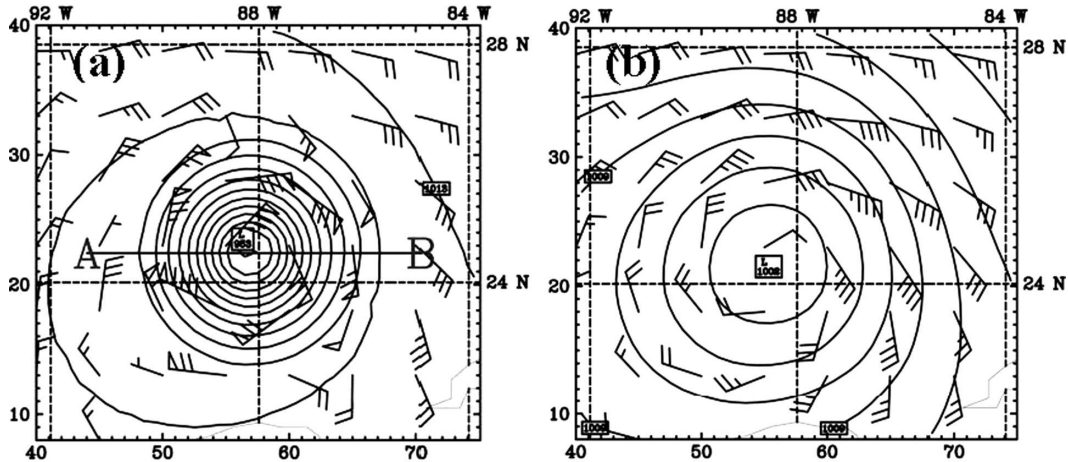


FIG. 16. The initial SLP (hPa) and model lowest level winds (m s^{-1}) of (a) 4DVAR6H1 and (b) CTRL at 1200 UTC 2 Oct 2002. The CSLP of (a) is 953 hPa.

(0000 UTC 3 October 2002), the hurricane CSLP is 945 hPa, which is only 4 hPa weaker than observed (Fig. 19a). The inner warm and moist cores are still maintained at lower levels. However, the hurricane's inner core has experienced some major changes. The temperature asymmetry aloft is larger than in Fig. 18b, with ranges of 2.3° – 3.0°C above 800 hPa (Fig. 19b). The moisture distribution has also become more uneven (Fig. 19c). The surface air is drier on the west side versus the east side by roughly $1\text{--}2 \text{ g kg}^{-1}$, and the low-level moist air extends much farther eastward whereas it tends to tail-off on the west side. Moreover, the air is dryer aloft on the west side; for example, the isopleths curve downward on the west side between 800 and 950 hPa, whereas they are smooth on the east side, representative of a moist environment in the low-level eastern eyewall sector. The result is an “open” eyewall,

with an outward sloping updraft in the eastern eyewall but subsidence west of the eye (Fig. 19d).

d. Hurricane intensity change in the 12-h 4DVAR cycling

Figure 20 presents the temporal variation of hurricane CSLP in the entire 12-h 4DVAR cycling assimilation window from 1200 UTC 2 October to 0000 UTC 3 October 2002. At the initial time, the CSLP decreases to 953 hPa in 4DVAR6H1 from 1002 hPa in the background. However, the hurricane CSLP at the end of 4DVAR6H1 (1800 UTC 2 October 2002) is about 14 hPa higher than observed. Through the second assimilation cycle 4DVAR6H2, the CSLP is adjusted to 944 hPa at 1800 UTC, 3 hPa higher than observed at this time. At the end of the assimilation window of 4DVAR6H2, the CSLP is 945 hPa, close to the obser-

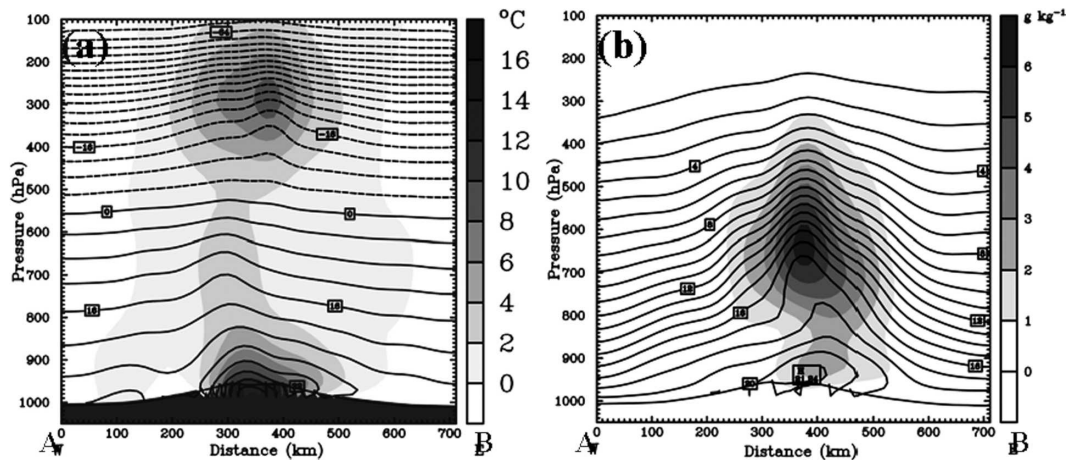


FIG. 17. Cross sections of (a) temperature (contour) and temperature difference from the MM5 background (shading, $^{\circ}\text{C}$), (b) specific humidity (solid line) and its difference from the CTRL (shading, g kg^{-1}) of Hurricane Lili after 4DVAR6H1 at 1200 UTC 2 Oct 2002.

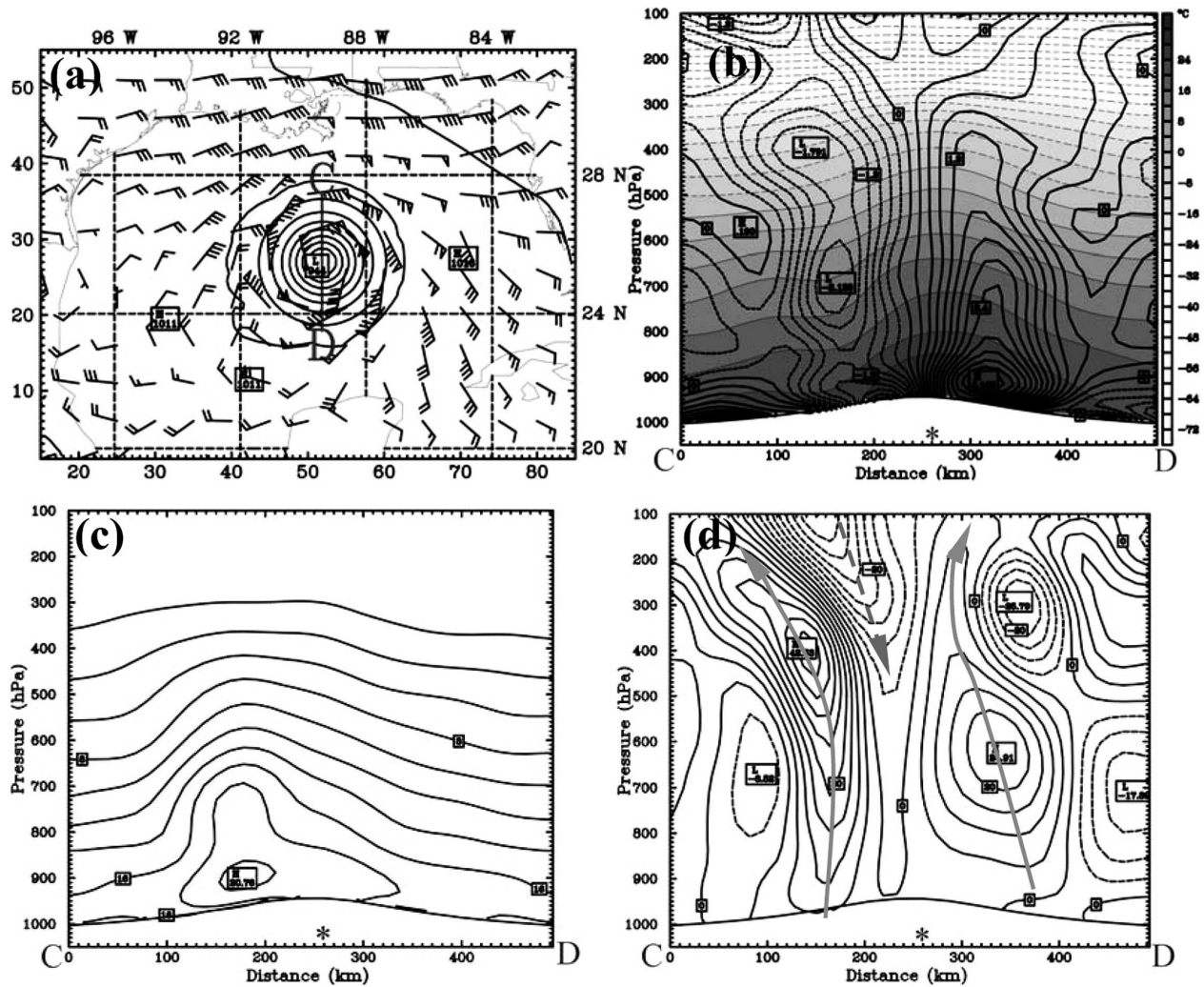


FIG. 18. Initial condition of 4DVAR6H2 at 1800 UTC 2 Oct 2002: (a) SLP (hPa) and lowest level horizontal winds (m s^{-1}); north-south cross section along the line CD for (b) temperature ($^{\circ}\text{C}$, shading with thin contours) and its deviation from azimuthal average ($^{\circ}\text{C}$, thick contours), (c) specific humidity (g kg^{-1}), and (d) vertical velocity (cm s^{-1}). The horizontal axis represents the distance from C in (a), and the asterisk shows the position of the hurricane's center.

vation (940 hPa). In comparison, the CTRL experiment without any bogusing and data assimilation has a CSLP of 996 hPa at this time.

e. Simulation results of Lili's rapid weakening phase

A triply nested MM5 simulation was used to model Hurricane Lili's weakening. A 24-h model integration was performed starting from 0000 UTC 3 October 2002 with the optimal initial condition of 4DVAR6H2. This numerical simulation is labeled SATC. To examine the satellite data impact on the simulation, another two simulations were conducted using only BDA in the 4DVAR cycling (labeled as BDAC) and using only satellite data in the 4DVAR cycling (labeled as SATO), respectively.

Figure 21 shows a time series of the hurricane's CSLP and low-level maximum winds. The initial intensity for SATC is closer to the observed than BDAC. Moreover, the SATC simulation experiences profound intensity changes in the first 6 h of the simulation. The CSLP increases from 945 to 960 hPa from 0000 to 0600 UTC 3 October 2002, followed by a much slower CSLP increase to 961 hPa on 1200 UTC; this matches the observed CSLP trend (Fig. 21a). In contrast, the BDAC's CSLP remains constant the first 6 h, then increases to 954 hPa on 1200 UTC, 8 hPa larger than observed. However, the maximum sustained wind speed comparisons do not produce exactly similar results (Fig. 21b). SATC also experiences rapid wind speed decreases during the first 6 h (from 69 to 42 m s^{-1}), then remains constant. However, the observed winds decrease at a

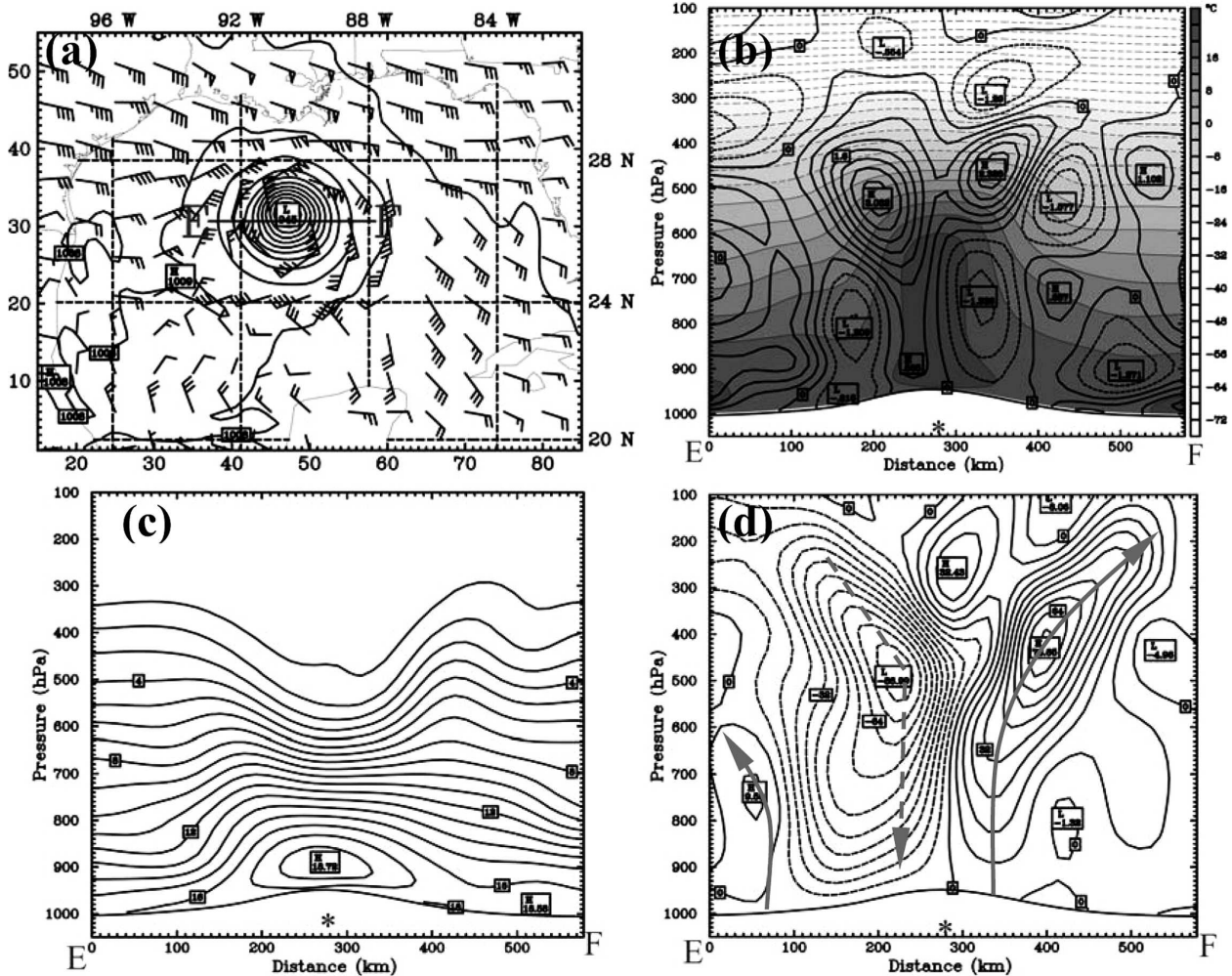


FIG. 19. Same as in Fig. 18, but at 0000 UTC 3 Oct 2002 (the end of the assimilation window of 4DVAR6H2) and with a west–east cross section [Line EF in (a)]. (a) The horizontal axis represents the distance from E and the asterisk shows the position of the hurricane’s center.

slower, steady rate (from 64 to 55 m s^{-1}) in the first 6 h, then to 41 m s^{-1} at 1200 UTC. This is an example of how tropical cyclone wind changes do not always correlate to rapid pressure changes, a situation observed often in these storms, and is indicative of the complicated dynamics involved. The BDAC simulation does show a steady wind speed decrease, but at a rate slower than observed. After landfall, both CTRL and SATC match the observed wind well, but the CSLP increase too slowly in both cases, mostly because the landfall is 5 h too late (see below).

In comparison, the CTRL is in error by more than 50 hPa at the initial time, so it is unable to forecast the weakening process. Moreover, it has an unrealistic intensification prior to landfall. SATO has a weakening trend after Lili’s landfall, but it is similar to CTRL during the first 9 h. Overall, vortex bogusing is necessary to

simulate the hurricane intensity change. If vortex bogusing is included in the 4DVAR cycling, satellite data—particularly the *Aqua* thermodynamic information—makes an immediate impact beyond normal bogusing procedures. The thermodynamic factors from *Aqua* contributing to this 6-h intensity decrease will be discussed more in the next section. The necessity of bogusing also suggests that inner-core wind information is a valuable area for future 4DVAR research with regard to intensity issues.

The 24-h SATC and BDAC predictions of the hurricane tracks are improved compared to the CTRL experiment, which contains no data assimilation and no bogusing (Fig. 22). CTRL moves slower than observed, and does not make landfall until 0000 UTC 4 October 2002, 11 h later than observed. Moreover, the forecasted track of CTRL has a notable westward bias dur-

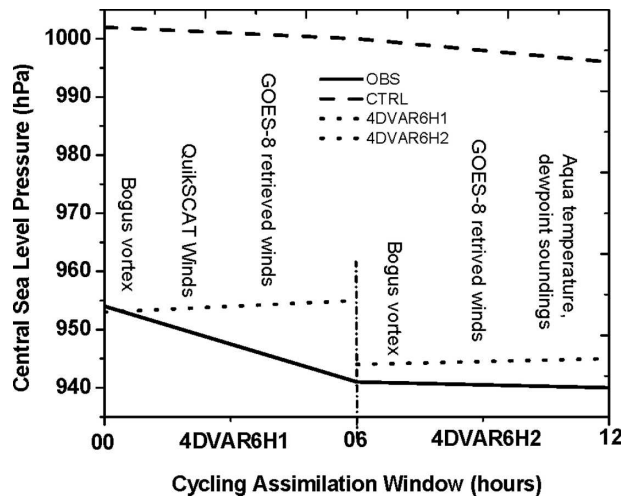


FIG. 20. Variations of CSLP (hPa) analyzed by 4DVAR cycling experiment (dot-dash), CTRL (dash), and the observation (solid).

ing the entire weakening period. When satellite data are included, the track of SATO is improved compared with CTRL. The movement speed and the track of SATO are much closer to OBS than CTRL, albeit the initial position does not change. The SATC and BDAC tracks are closer to the observed, and move faster than CTRL. Comparing SATC with BDAC, the impact of the satellite data is still evident, as the SATC track prediction is closer to the observed than BDAC, although both in general handle the landfall location reasonably well. However, the landfall timing for both simulations is about 1800 UTC 3 October 2002, 5 h later than the observation.

f. Analyses of dry air intrusion during Lili's weakening

Based on the SATC results, one probable reason behind Hurricane Lili's quick weakening is examined. Many factors can cause a hurricane to weaken over the ocean, such as cooler sea surface temperature (SST), strong winds shear aloft, and dry air intrusion. Jin and Liou's (2004) modeling results concluded that neither SST cooling nor wind shear were the major factors leading to Hurricane Lili's quick demise. Future 4DVAR research will examine these possibilities further. Because of the obvious influence of the MODIS thermodynamic data in the 4DVAR runs, the impact of dry air intrusion will be examined in this paper.

Figure 23 shows the difference in mixing ratio fields between 4DVAR6H2 and 4DVAR6H1 at 1800 UTC 2 October and 0000 UTC 3 October 2002. Negative difference exists at 950 and 300 hPa at 1800 UTC (Figs. 23a,b), signifying drier air than the 4DVAR6H1 first guess after including the *Aqua* MODIS sounding data.

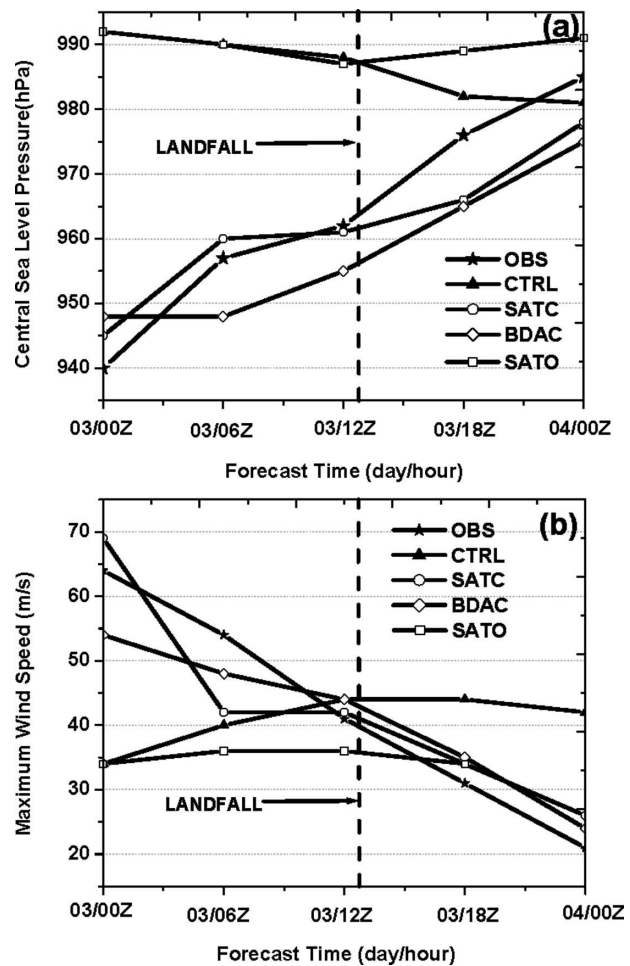


FIG. 21. Predicted (a) CSLP (hPa) and (b) maximum low-level wind speed ($m s^{-1}$) from 0000 UTC 3 Oct to 0000 UTC 4 Oct 2002 from 1) model background with no data assimilation [CTRL (triangle)]; 2) 4DVAR data assimilation of vortex bogusing and satellite data from QuikSCAT surface winds, *GOES-8* upper-level winds, and *Aqua* soundings, [SATC (circle)]; and 4DVAR with bogusing only [BDAC (diamond)]; and 4DVAR with satellite data only [SATO (square)]. Observed is also shown (pentagon). Landfall occurred on 1300 UTC 3 Oct 2002.

The 300-hPa mixing ratio is only minimally less ($<1 g kg^{-1}$) at the end of each cycle west and south of the hurricane, but the 950-hPa air is significantly drier to the west and south, reducing mixing ratio values by 4–7 $g kg^{-1}$ (Figs. 23c,d). The dry air propagates cyclonically toward the hurricane center from its southwest quadrant, as seen at 0000 UTC 3 October 2002 at the end of 4DVAR6H2 (Figs. 23b,d). This corresponds to the time when the western updraft weakened in the eyewall (Fig. 19d). Therefore, this dry air intrusion might contribute to the rapid weakening starting 0000 UTC 3 October 2002.

One can argue that the dry surface air on the west side of Lili caused an open eyewall, with subsidence

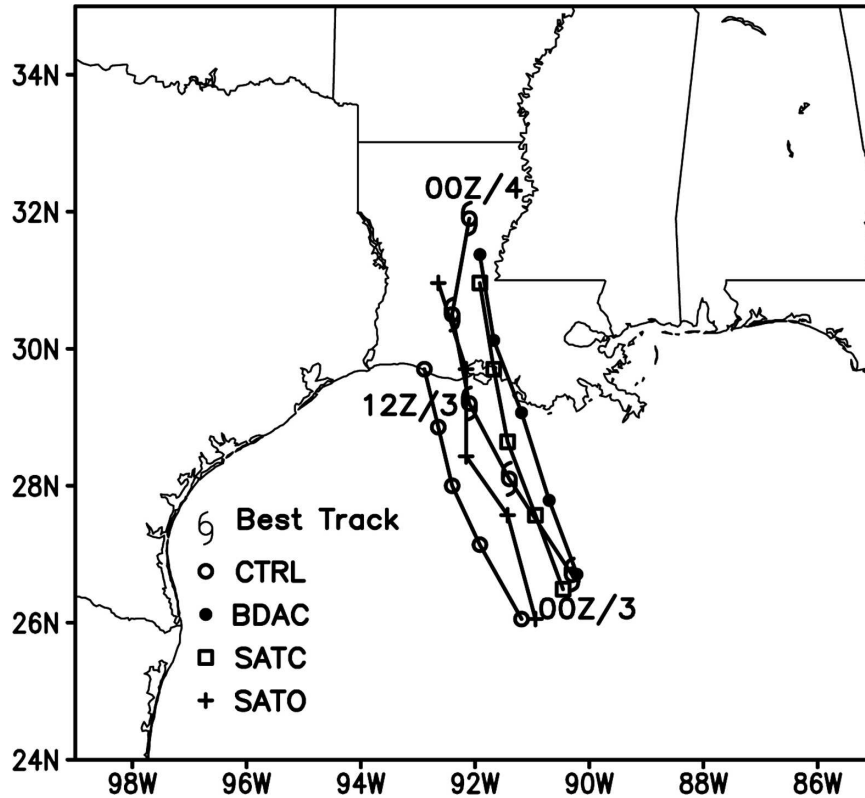


FIG. 22. The predicted track of Hurricane Lili (2002) by CTRL, SATC, BDAC, SATO, and the observed best track from 0000 UTC 3 Oct to 0000 UTC 4 Oct 2002.

west of the eye (Fig. 19d). An open eye was observed at 0900 UTC 3 October 2002 as stated in the 0500 EDT National Hurricane Center discussion: "Aircraft flight-level and dropsonde data indicate that Lili has weakened significantly since reaching its peak intensity yesterday evening. The Hurricane Hunters reported that the eyewall has collapsed into a few fragments . . . however WSR-88D from New Orleans and Lake Charles still show about 50% of an eyewall . . . open to the south." The weakening of Hurricane Lili was associated with a collapsing eyewall, and this suggests dry air intrusion played a component in the storm's rapid weakening.

Mean relative humidity (MRH) values 200 km from the storm center also support this hypothesis. Values from 1800 UTC 2 October to 0600 UTC 3 October 2002 are shown in Table 3 at model levels $\sigma = 0.9735$, 0.9615, and 0.9475. Low-level MRH values decrease during this 12-h period. At 1800 UTC 2 October 2002, the MRH is more than 90%. The dry air at this time is far from the hurricane center area (Fig. 23a). Six hours later, the MRH is reduced by more than 10% at each level, which illuminates that dry air has propagated into the hurricane center. The dry air intrusion is also shown in Fig. 23b. MRH continues to decrease at 0600 UTC 3 October 2002, indicating increased dry air encroachment.

An examination of the SATC and BDAC 850-hPa relative humidity fields at 0000 UTC 3 October 2002 also supports this assertion (Fig. 24). The BDAC experiment shows a fairly symmetric relative humidity field (Fig. 24a), while the SATC 0000 UTC field shows the inner-core becoming disorganized, with saturated fields confined to the east and north (Fig. 24b). The differences are dramatic, with relative humidity differences up to 50% on the southwest side (Fig. 24c). The dry air also reduced the surface temperature through wet bulb processes (not shown). The SATC vortex also had a warmer inner core above 700-hPa due to a better-defined circulation (Fig. 23). Both these factors, combined with less available low-level moisture, reduced parcel buoyancy in the eyewall, inhibiting convection. It is concluded that low-level dry air intrusion was a major factor in Lili's rapid weakening by causing entrainment and by inhibiting eyewall convection on the west and south side.

7. Summary and conclusions

MM5 4DVAR sensitivity runs were conducted separately with QuikSCAT surface winds, GOES-8 cloud

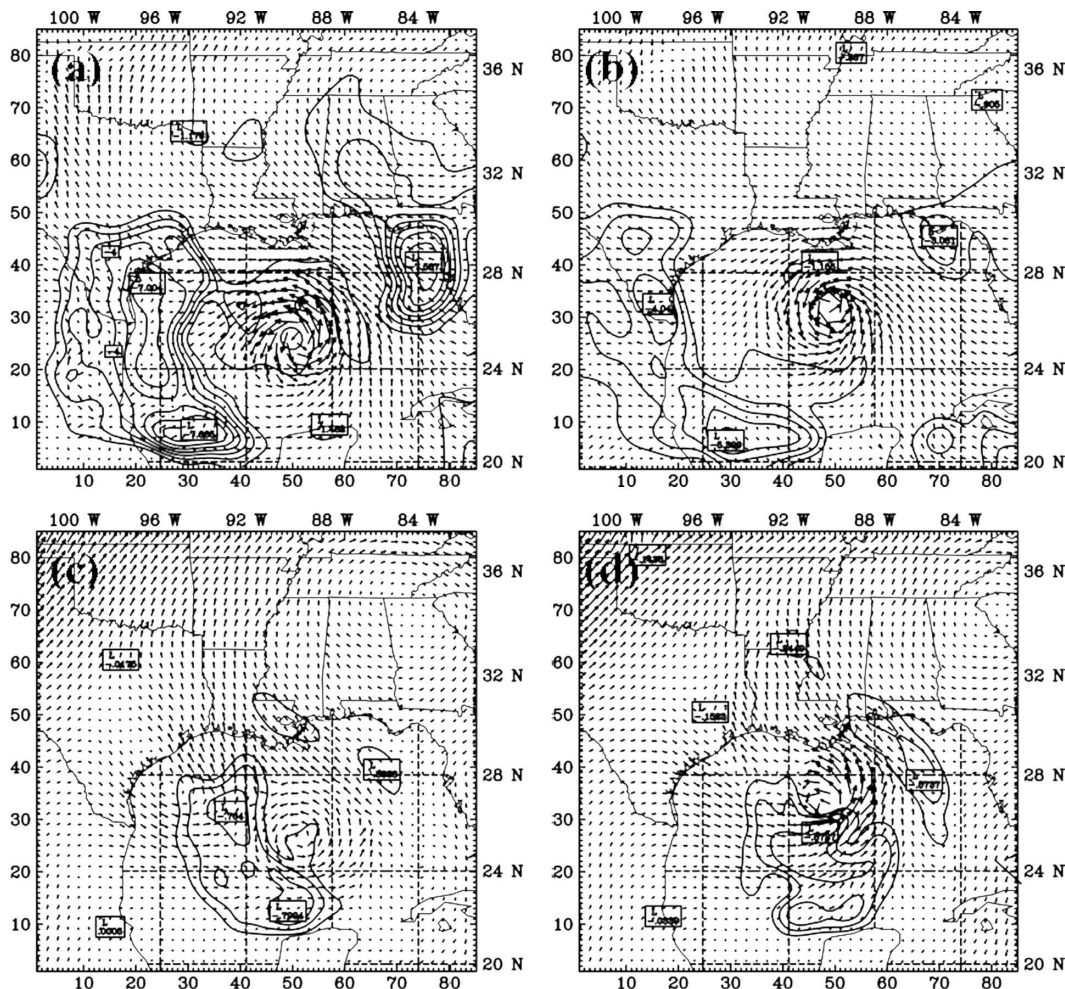


FIG. 23. Difference (4DVAR6H2 minus 4DVAR6H1) of water vapor mixing ratio (solid line, g kg^{-1}) and wind vector (m s^{-1}) at 950 hPa for (a) 1800 UTC 2 Oct and (b) 0000 UTC 3 Oct 2002; and at 300 hPa for (c) 1800 UTC 2 Oct and (d) 0000 UTC 3 Oct 2002.

drift–water vapor winds, and *Aqua* MODIS temperature–dewpoint soundings to investigate their individual impact on storm track and intensity. The results were compared against a simulation initialized from a GFS background interpolated to the MM5 grid. The following conclusions emerged:

- Assimilating QuikSCAT surface wind data improves the analysis outer-core surface winds, as well as the inner-core low-level temperature and moisture fields.
- Substantial adjustments of winds are noted in certain regions on the periphery of the hurricane by assimilating *GOES-8* satellite-derived upper-level winds.
- Both track forecasts initialized at 1200 UTC 2 October 2002 with 4DVAR of QuikSCAT and *GOES-8* show improvement compared to those initialized with the model background. However, the inner-core wind analysis is still too weak, so the intensity prediction cannot be improved.

- Assimilating *Aqua* MODIS sounding data improves the outer-core thermodynamic features. In particular, the low-level moisture field west of the hurricane is drier than the background field. The *Aqua* MODIS data has little impact on the track forecast, but does show evidence of impacting the model intensity predicting by retarding the incorrect prediction of intensification.

To properly investigate Lili’s rapid weakening, a bogus vortex is necessary in the 4DVAR iterative pro-

TABLE 3. MRH 200-km from the hurricane’s center.

Level RH%	1800 UTC 2 Oct	0000 UTC 3 Oct	0600 UTC 3 Oct
$\sigma = 0.9735$	99.74379	87.4904	83.05276
$\sigma = 0.9615$	96.30346	80.87632	75.13392
$\sigma = 0.9475$	90.29882	74.29162	73.94376

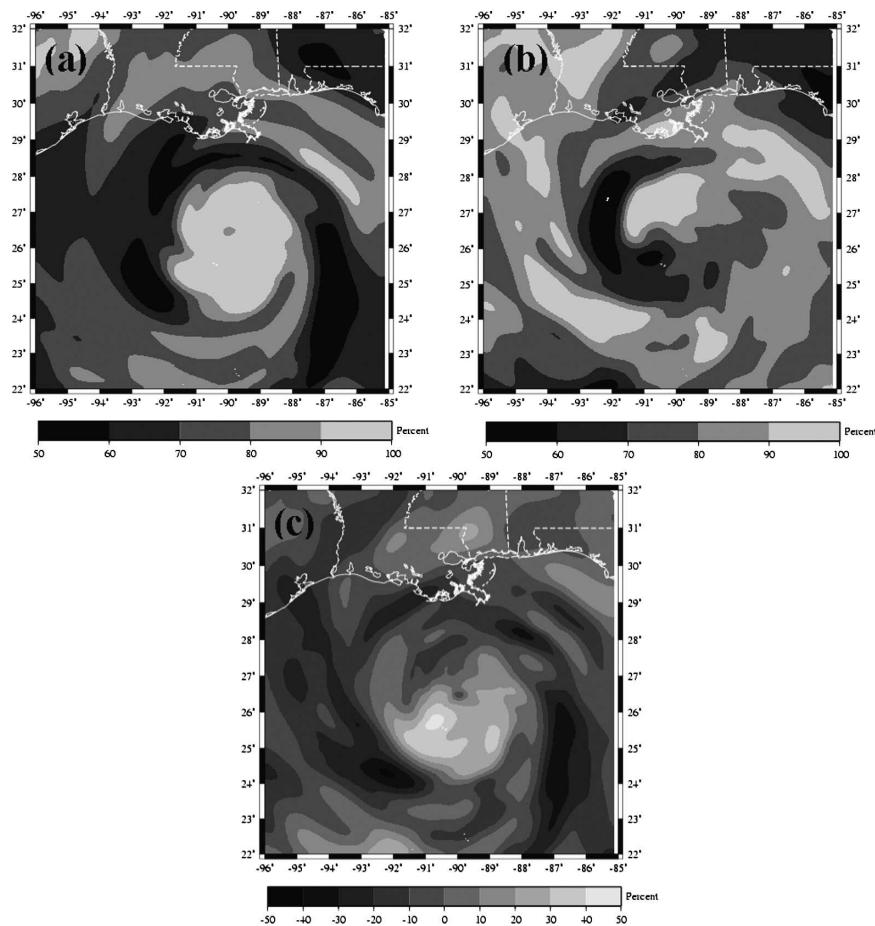


FIG. 24. The 850-hPa relative humidity in domain C at 0000 UTC 3 Oct 2002 for (a) BDAC and (b) SATC. (c) The difference computed as BDAC minus SATC.

cess so that the model initialization matches the observed intensity at 0000 UTC 3 October 2002. A data assimilation experiment, which combines BDA, QuikSCAT winds, *GOES-8* winds, and *Aqua* MODIS soundings data, is performed to investigate Lili's weakening phase. The 4DVAR data assimilation is conducted in two consecutive 6-h assimilation windows preceding Lili's weakening. Results show that significant differences among experiments with initial conditions derived from 1) CTRL without 4DVAR assimilation of any satellite data and bogus vortex; 2) 4DVAR cycling experiment with BDA, QuikSCAT winds, *GOES-8* cloud drift/water vapor winds, and *Aqua* MODIS sounding data; and 3) 4DVAR cycling with BDA only (satellite data were denied). The numerical results led to the following conclusions.

- The satellite data—particularly the *Aqua* thermodynamic information—makes an immediate impact on the hurricane intensity beyond normal bogussing pro-

cedures. The satellite data assimilation experiment using MM5 4DVAR cycling mode dramatically weakens both CSLP and maximum surface winds in the first 6 h after 0000 UTC 3 October 2002, while the 4DVAR with BDA keeps CSLP intensity constant for the first 6 h, and decreases winds slower than observed the first 6 h. The track forecast with the satellite data is also more accurate than just using bogussing alone.

- The low-level air on the hurricane's west side is drier after including the *Aqua* MODIS sounding data in 4DVAR. This drier air propagates toward the hurricane center from the southwest quadrant. Cross-section plots show this dry air resulting in a weaker updraft in the southern eyewall at 1800 UTC 2 October 2002, and an open western eyewall with subsidence at 0000 UTC 3 October 2002, when the hurricane begins to rapidly weaken. The BDAC analysis at this time shows a fairly symmetric low-level relative humidity field, while the SATC 0000 UTC field

shows the inner-core becoming disorganized, with saturated fields confined to the east and north. These results suggest low-level dry air intrusion was a major factor in Lili's rapid weakening by causing entrainment and by inhibiting eyewall convection on the west and south side.

This study demonstrates the potential benefit of using satellite data in a 4DVAR context, particularly high-resolution soundings, on unusual cases like Hurricane Lili. Future issues include studying the impact of hurricane reconnaissance data so as to capture the actual hurricane inner-core winds instead of bogusing them. Research on the direct assimilation of the satellite radiance data instead of soundings retrievals also contains certain advantages, as does the usage of precipitable water. Finally, continued progress in computational power with the development of parallel 4DVAR code will greatly enhance the ability to perform tropical cyclone intensity studies with these cutting edge data sources.

Acknowledgments. We are very grateful to G. Holland and Y.-H. Kuo for their support, encouragement, and suggestions for this work. The QuikSCAT data is courtesy of Remote Sensing Systems, Inc. The *GOES-8* winds were provided by Chris Velden of the Cooperative Institute for Meteorological Satellite Studies at the University of Wisconsin—Madison. The *Aqua* MODIS data was supplied by the NASA Goddard Earth Sciences (GES) Data and Information Services Center (DISC) via the GES Distributed Active Archive Center (DAAC). We are in debt to V. Anantharaj, Y. Lau, S. Bhat, and N. Tran who preprocessed the satellite data, and to Z. Ma who provided his expertise in our data assimilation experiments. This research could not have been conducted without their assistance. Comments of the initial draft of this work by X.-Y. Huang and Y. Chen greatly improve the presentation of the paper. Suggestions by the reviewers facilitated a more comprehensive paper. The authors also thank WorldWinds, Inc. for supporting this work, and providing matching funds and programming expertise. This research is supported by the awards of NOAA 05111076, NASA through the University of Mississippi's Enterprise for Innovative Geospatial Solutions under the terms of Agreement NAG13-03012, and NASA Grant NCC13-99001.

REFERENCES

- Bennett, A. F., L. M. Leslie, C. R. Gagelberg, and P. E. Powers, 1993: Tropical cyclone prediction using a barotropic model initialized by a generalized inverse method. *Mon. Wea. Rev.*, **121**, 1714–1729.
- , B. S. Chua, and L. M. Leslie, 1996: Generalized inversion of a global numerical weather prediction model. *Meteor. Appl. Phys.*, **60**, 165–178.
- Brown, R. A., and L. Zeng, 1994: Estimating central pressures of oceanic midlatitude cyclones. *J. Appl. Meteor.*, **33**, 1088–1095.
- Dowell, C. D., F. Zhang, L. J. Wicker, C. Snyder, and N. A. Crook, 2004: Wind and temperature retrievals in the 17 May 1981 Arcadia, Oklahoma, supercell: Ensemble Kalman filter experiments. *Mon. Wea. Rev.*, **132**, 1982–2005.
- Elliott, W. P., and D. J. Gaffen, 1993: Effects of conversion algorithms on reported upper-air dewpoint depressions. *Bull. Amer. Meteor. Soc.*, **74**, 1323–1325.
- Elsberry, R. L., 1990: International experiments to study tropical cyclones in the western North Pacific. *Bull. Amer. Meteor. Soc.*, **71**, 1305–1316.
- Evensen, G., 1994: Sequential data assimilation with a nonlinear quasi-geostrophic model using Monte Carlo methods to forecast error statistics. *J. Geophys. Res.*, **99** (C5), 10 143–10 162.
- Frederick, W. J., 2003: The rapid intensification and subsequent rapid weakening of Hurricane Lili as compared with historical hurricanes. *Wea. Forecasting*, **18**, 1295–1298.
- Fujita, T., 1952: Pressure distribution within a typhoon. *Geophys. Mag.*, **23**, 437–451.
- Graf, J., C. Sasaki, C. Winn, W. T. Liu, W. Tsai, M. Freilich, and D. Long, 1998: NASA scatterometer experiment. *Astrophys. J.*, **43**, 397–407.
- Guo, Y.-R., Y.-H. Kuo, J. Dudhia, D. Parsons, and C. Rocken, 2000: Four-dimensional variational data assimilation of heterogeneous mesoscale observations for a strong convective case. *Mon. Wea. Rev.*, **128**, 619–643.
- Hack, J. J., and W. H. Schubert, 1986: Nonlinear response of atmospheric vortices to heating by organized cumulus convection. *J. Atmos. Sci.*, **43**, 1559–1573.
- Holmlund, K., S. V. Christopher, and R. Michael, 2001: Enhanced automated quality control applied to height-density satellite-derived winds. *Mon. Wea. Rev.*, **129**, 517–529.
- Jin, Y., and C.-S. Liou, 2004: A numerical model investigation of intensity forecast errors for Hurricane Lili (2002). Preprints, *20th Conf. on Weather Analysis and Forecasting/16th Conf. on Numerical Weather Prediction*, Seattle, WA, Amer. Meteor. Soc., CD-ROM, 3.2a.
- Katsaros, K. B., E. B. Forde, P. Chang, and W. T. Liu, 2001: QuikSCAT's SeaWinds facilitates early identification of tropical depressions in 1999 hurricane season. *Geophys. Res. Lett.*, **28**, 1043–1046.
- King, M. D., and Coauthors, 2003: Cloud and aerosol properties, precipitable water, and profiles of temperature and water vapor from MODIS. *IEEE Trans. Geosci. Remote Sens.*, **41**, 442–458.
- Kuo, Y.-H., S. Sokolovskiy, R. A. Anthes, and F. Vandenberghe, 2000: Assimilation of GPS radio occultation data for numerical weather prediction. *TAO*, **11**, 157–186.
- Leidner, S. M., L. Isaksen, and R. N. Hoffman, 2003: Impact of NSCAT winds on tropical cyclones in the ECMWF 4DVAR assimilation system. *Mon. Wea. Rev.*, **131**, 3–26.
- Le Marshall, J. F., W. Smith, and G. Gallan, 1985: Hurricane Debby—An illustration of the complementary nature of VAS soundings and cloud and water vapor motion winds. *Bull. Amer. Meteor. Soc.*, **66**, 258–263.
- , L. M. Leslie, and C. Spinoso, 1996: The impact of spatial and temporal distribution of satellite observations on tropical cyclone data assimilation: Preliminary results. *Meteor. Atmos. Phys.*, **60**, 157–163.

- Leslie, L. M., and G. J. Holland, 1995: On the bogussing of tropical cyclones in numerical models: A comparison of vortex profiles. *Meteor. Atmos. Phys.*, **56**, 101–110.
- , J. F. Le Marshall, R. P. Morison, C. Spinoso, R. J. Purser, N. Pescod, and R. Seecamp, 1998: Improved hurricane track forecasting from the continuous assimilation of high quality satellite wind data. *Mon. Wea. Rev.*, **126**, 1248–1257.
- Menzel, W. P., S. W. Seaman, J. Li, and L. E. Gumley, 2002: MODIS atmospheric profile retrieval algorithm theoretical basis document. CIMSS Tech. Rep., 35 pp. [Available from CIMSS, Space Science and Engineering Center, University of Wisconsin—Madison, 1225 West Dayton St., Madison, WI 53706.]
- Mills, G. A., G. M. Gallan, and B. M. Goodman, 1986: A meso-scale data assimilation scheme for real time use in the McIDAS environment. CIMSS Tech. Rep., 86 pp. [Available from CIMSS, Space Science and Engineering Center, University of Wisconsin—Madison, 1225 West Dayton St., Madison, WI 53706.]
- Pu, Z.-X., and S. A. Braun, 2001: Evaluation of bogus vortex techniques with four-dimensional variational data assimilation. *Mon. Wea. Rev.*, **129**, 2023–2039.
- , W.-K. Tao, S. Braun, J. Simpson, Y. Jia, J. Halverson, W. Olson, and A. Hou, 2002: The impact of TRMM data on mesoscale numerical simulation of Supertyphoon Paka. *Mon. Wea. Rev.*, **130**, 2448–2458.
- Reisner, J., R. J. Rasmussen, and R. T. Bruintjes, 1998: Explicit forecasting of supercooled liquid water in winter storms using the MM5 mesoscale model. *Quart. J. Roy. Meteor. Soc.*, **124B**, 1071–1107.
- Soden, B., C. S. Velden, and R. Tuleya, 2001: The impact of satellite winds on experimental GFDL hurricane model forecasts. *Mon. Wea. Rev.*, **129**, 835–852.
- Velden, C., C. Hayden, W. Menzel, J. L. Franklin, and J. S. Lynch, 1992: The impact of satellite-derived winds on numerical hurricane track forecasts. *Wea. Forecasting*, **7**, 107–118.
- , T. Olander, and S. Wanzong, 1998: The impact of multi-spectral GOES-8 wind information on Atlantic tropical cyclone track forecasts in 1995. Part I: Dataset methodology, description, and case analysis. *Mon. Wea. Rev.*, **126**, 1202–1218.
- Xiao, Q., X. Zou, and Y.-H. Kuo, 2000a: Incorporating the SSM/I-derived precipitable water and rainfall rate into a numerical model: A case study for the ERICA IOP-4 cyclone. *Mon. Wea. Rev.*, **128**, 87–108.
- , —, and B. Wang, 2000b: Initialization and simulation of a landfalling hurricane using a variational bogus data assimilation scheme. *Mon. Wea. Rev.*, **128**, 2252–2269.
- , —, M. Ponca, M. A. Shapiro, and C. Velden, 2002: Impact of GMS-5 and GOES-9 satellite-derived winds on the prediction of a NORPEX extratropical cyclone. *Mon. Wea. Rev.*, **130**, 507–528.
- Xue, M., M. Tong, and K. K. Droegemeier, 2006: An OSSE framework based on the ensemble square root Kalman filter for evaluating the impact of data from radar networks on thunderstorm analysis and forecasting. *J. Atmos. Oceanic Technol.*, **23**, 46–66.
- Zhang, X.-Y., B. Wang, Z. Ji, Q. Xiao, and X. Zhang, 2003: Initialization and simulation of a typhoon using 4-dimensional variational data assimilation—Research on Typhoon Herb (1996). *Adv. Atmos. Sci.*, **20**, 612–622.
- Zhao, Y., B. Wang, Z. Ji, X. Liang, G. Deng, and X. Zhang, 2005: Improved track forecasting of a typhoon reaching landfall from four-dimensional variational data assimilation of AMSU-A retrieved data. *J. Geophys. Res.*, **110**, D14101, doi:10.1029/2004JD005267.
- Zhu, T., D.-L. Zhang, and F. Weng, 2002: Impact of the Advanced Microwave Sounding Unit measurements on hurricane prediction. *Mon. Wea. Rev.*, **130**, 2416–2432.
- Zou, X., and Q. Xiao, 2000: Studies on the initialization and simulation of a mature hurricane using a variational bogus data assimilation scheme. *J. Atmos. Sci.*, **57**, 836–860.
- , W. Huang, and Q. Xiao, 1998: A user's guide to the MM5 adjoint modeling system. NCAR Tech. Note TN-437+IA, NCAR/MMM Division, 92 pp. [Available from NCAR Publications Office, P.O. Box 3000, Boulder, CO 80307-3000.]
- , Q. Xiao, A. E. Lipton, and G. D. Modica, 2001: A numerical study of the effect of GOES sounder cloud-cleared brightness temperatures on the prediction of Hurricane Felix. *J. Appl. Meteor.*, **40**, 34–55.